High-throughput analysis by NIR spectroscopy for efficient bioethanol production

(Laboratory of Biomass Morphogenesis and Information, RISH, Kyoto University)

Yoshiki Horikawa, Tomoya Imai and Junji Sugiyama

Near-infrared (NIR) spectroscopy is a nondestructive, fast, and accurate measurement for analyzing chemical components on the basis of overtone and combination bands of specific functional groups. Recently, NIR spectroscopy combined with multivariate statistics has provided chemometric tools such as principal components analysis (PCA) and partial least squares (PLS) regression methods. The former is available for grouping the samples involving similar properties and identifying the specific spectral features. The latter can build the model relationships between large numbers of dependent variables containing complex variations as NIR spectra and independent variations. PLS regression has been particularly successful in creating calibration model for predicting chemical components and physical features, which allows high-throughput analysis.

We applied this technique to quantify individual chemical components of pretreated biomass alternative to the wet chemical method, which is labor-intensive, expensive, and time consuming. Furthermore, the performance of enzymatic hydrolysis for exhaustive biomass was successfully evaluated by above-mentioned chemometric approach. NIR has a great potential for rapid screening of saccharification efficiency of pretreated biomass, which would allows us to control the quality of processing toward better bioethanol production.
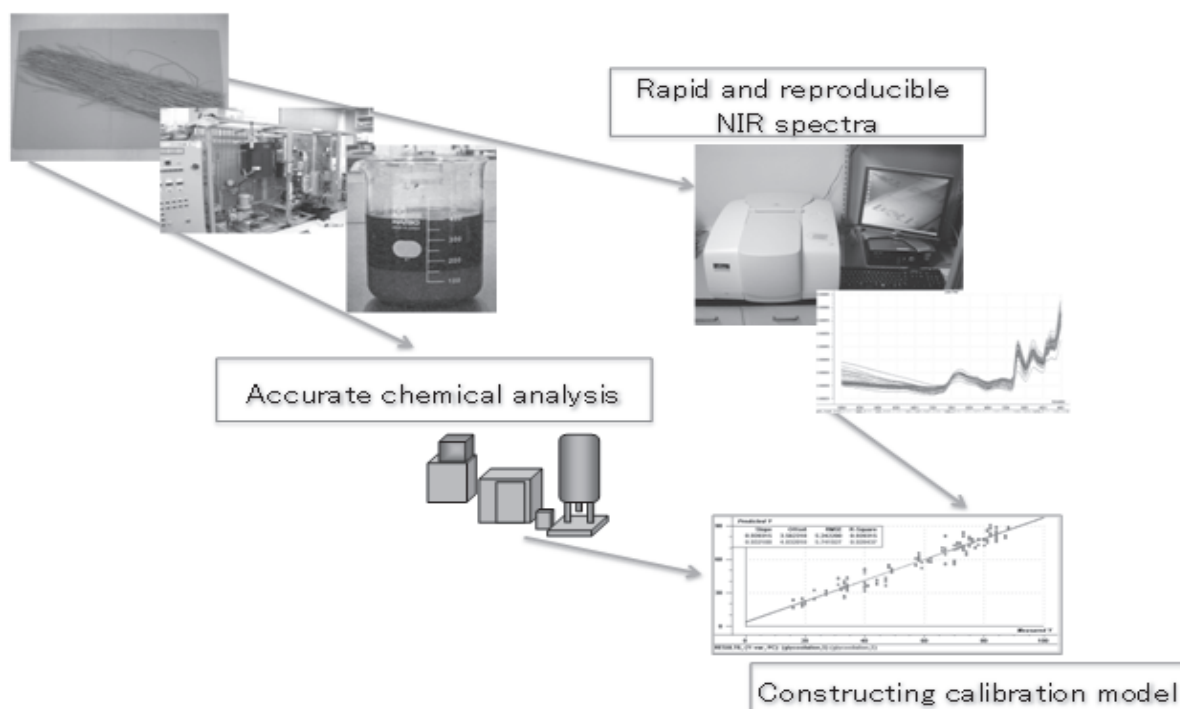

Figure Schematic illustration of the procedure to construct the calibration model between the wet chemical data and the NIR spectral data.

Research on molecular relationship between fatty acid metabolism and selective lignin degradation in *Ceriporiopsis subvermispora*

(Laboratory of Biomass Conversion, RISH, Kyoto University)

Takahito Watanabe, Yoichi Honda, and Takashi Watanabe

Ceriporiopsis subvermispora, a white-rot fungus, is characterized as one of the best bio-pulping fungi because it can selectively degrade lignin without serious damage to cellulose. We have demonstrated that the same fungus produces large amounts of unsaturated fatty acids (UFAs), such as linoleic acid (18:2n-6), and degrades lignin by manganese peroxidase-catalyzed lipid peroxidation (LPO). In spite that UFAs might act as precursors of LPO, however, the molecular relationship between UFA biosynthesis and lignin degradation in white-rot fungi including *C. subvermispora* has remained to be elucidated; therefore, we focused on UFAs, linoleic acid in particular, which is a potential precursor of LPO involved in the selective lignin degradation by *C. subvermispora*.

Firstly, we have cloned a cDNA fragment containing one open reading frame (ORF) using the PCR-based methods. This ORF product had similarities with various fungal Δ12-fatty acid desaturases, which converts oleic acid (18:1n-9) to linoleic acid. The same product had three histidine cluster motifs (His-box), which are known to be the consensus sequence of fatty acid desaturases. Using the SOSUI system to classify and predict the secondary structure of membrane proteins, moreover, this ORF product was estimated to be a membrane-bound protein with four transmembrane helices. These observations strongly suggested that this ORF encodes a Δ12-fatty acid desaturase in *C. subvermispora*. We designated this ORF as *Cs-fad2*.

For heterologous expression of *Cs-fad2*, we constructed an expression plasmid in which *Cs-fad2* cDNA was oriented to a constitutive promoter of the alcohol dehydrogenase 1 gene (*ADH1*). After transformation of the expression plasmid in budding *Saccharomyces cerevisiae* lacking a Δ12-fatty acid desaturase gene, we performed fatty acid analysis of the yeast transformant carrying *Cs-fad2*. A single peak in the chromatogram of gas chromatography analysis was detected specifically for fatty acid methyl esters from the transformant and its retention time was identical to that of authentic methyl linoleate (C18:2). Gas chromatography–mass spectrometry analysis of the fatty acid methyl derivative demonstrated that its mass peak was at *m/z* 294, the same molecular mass methyl linoleate, and that the fragmentation pattern was identical to that of authentic standard of methyl linoleate. These results indicated that the *Cs-fad2* gene encodes for *C. subvermispora* Δ12-fatty acid desaturase, which converts oleic acid to linoleic acid.

We also performed transcriptional analysis of *Cs-fad2* in various culture conditions. The transcription of *Cs-fad2* was activated and repressed in the presence of a lignin fragment like vanillin and exogenous fatty acids, respectively. Because vanillin is a key intermediate found during lignin biodegradation, the transcriptional activation of *Cs-fad2* by vanillin is very intriguing, and also seems to support our previous results that *C. subvermispora* produces large amounts of linoleic acid at an early stage of wood decay. These results may shed light on the molecular relationship between fatty acid metabolism and selective lignin degradation in *C. subvermispora*.

Reference

[1] Watanabe, T., Tsuda, S., Nishimura, H., Honda, Y., and Watanabe, T. (2010) Characterization of a Δ-12 fatty acid desaturase gene from *Ceriporiopsis subvermispora*, a selective lignin-degrading fungus. *Appl. Microbiol. Biotechnol.* 87: 215-224.

Inter-university Upper atmosphere Global Observation NETwork (IUGONET)

(Laboratory of Atmospheric Sensing and Diagnosis, RISH, Kyoto University)

Hiroo Hayashi

To investigate the mechanism of long-term variations in the upper atmosphere, we need to create integrated and organic links between various types of ground-based observation made at different locations and altitudes. The databases of such observations, however, have been maintained and made available to the community by each institution that conducted the observations. That is one reason that those data have been used only for studies of specific phenomena. For the same reason some of the observational data have been used by only a very few researchers who were involved in the observation campaign and have never been made available to other researchers.

A six-year research project, Inter-university Upper atmosphere Global Observation NETwork (IUGONET; http://www.iugonet.org/en/), was just initiated in 2009 to overcome such problems of data use by the five Japanese universities and institutes (Kyoto University, National Institute of Polar Research, Tohoku University, Nagoya University, and Kyushu University) that have been leading ground-based observations of the upper atmosphere for decades. We are collaborating to build a database system for the metadata of our observational data (Figure 1). Metadata, also known as meta-information, is "data about data"; that is, it describes the properties of data, such as the observation location and period, type of instrument, and data format. The metadata database (MDB) archiving this information will be of great help to researchers in efficiently finding and obtaining various observational data we have accumulated over many years. The MDB system will significantly facilitate the analyses of a variety of observational data, which we believe will lead to more comprehensive studies of the mechanisms of long-term variations in the upper atmosphere. Moreover, we expect that researchers will become familiar with not only data in their area of expertise but also data from different atmospheric regions by using the MDB. This will contribute to the promotion of new interdisciplinary studies regarding the upper atmosphere.
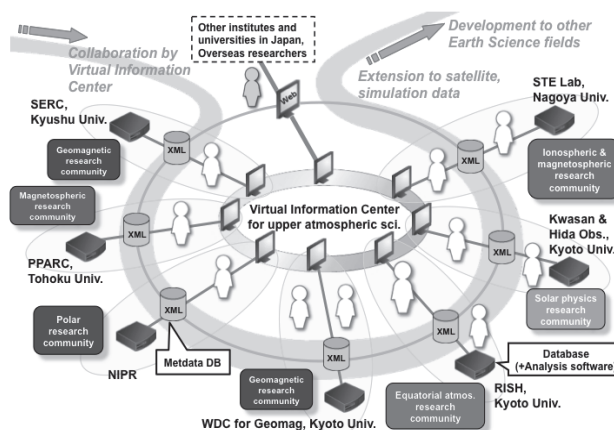

Figure 1. Schematic of the IUGONET project

The IUGONET development team, currently composed of 11 researchers representing each participating institution, have been frequently discussing at web and video conferences (about once per week) so far and has designed the initial version of our metadata format based on the Space Physics Archive Search and Extract (SPASE) data model, which is a metadata format developed by international consortium to comprehensively describe research resources regarding heliospheric and magnetospheric satellite observations. We have added some modifications depending on characteristics of our ground-based observations of the upper atmosphere. Creating metadata of our archived observational data according the metadata format is now underway. We have been working to build the MDB system on a free software named DSpace, which is widely used in many university digital repository. The development of integrated data analysis and plotting tool for our observational data (named UDAS – iUgonet Data Analysis Software) also just started, and it will be produced with the THEMIS Data Analysis Software (TDAS) Interactive Data Language (IDL) libraries and be functioned on the free, IDL Virtual Machine.

The IUGONET MDB and data analysis software (UDAS) are scheduled to be released to public in the fiscal year of 2011. Our project will be continued in order to further expand the system to other Earth science fields.

Kinetics of the atmospheric oxidation reaction of isoprene studied by pulsed laser photolysis / vacuum ultraviolet laser-induced fluorescence spectroscopy technique

(Laboratory of Atmospheric Environmental Information Analysis, RISH, Kyoto University)

Kenshi Takahashi

Isoprene is, by far, the most dominant volatile organic compound emitted into the Earth's atmosphere. Forests and plants emit approximately 500 TgC yr^{-1} of isoprene, while the combined emission of all volatile compounds from global transportation (land, water, and air) is approximately 22 TgC yr^{-1} [1]. A detailed understanding of the atmospheric oxidation mechanism of isoprene is clearly an important input for global atmospheric models. The atmospheric oxidation of isoprene is initiated by reaction with OH radicals, NO_3 radicals, and ozone. During daylight hours OH radicals likely dominate, while during nighttime the NO_3 radical is important. Evidence of relatively high concentrations of Cl atoms in the lower troposphere has prompted suggestions of the potential importance of Cl-initiated oxidation of isoprene.

To improve our understanding of the kinetics of Cl-initiated oxidation of isoprene, we employed absolute and relative rate methods to study this reaction in 1-700 Torr of N_2 and argon diluent [2]. Absolute rate measurements were made using pulsed laser photolysis / vacuum ultraviolet laser-induced fluorescence techniques (PLP/VUV-LIF). Relative rate measurements were made using smog chamber / FT-IR techniques. All experiments were performed at 297 ± 2 K. In the PLP/VUV-LIF experiments, gas mixtures of Cl_2 and isoprene diluted in N_2 or Ar were flowed through the reaction chamber. An excimer laser operating in a XeF mode generated 351 nm light to initiate the isoprene + Cl reaction through the photolytic production of Cl atoms from Cl_2 molecules. Cl($^2P_{3/2}$) atoms were detected by VUV-LIF at 134.72 nm at $3p^5$ $^2P_{3/2}$ - $4p^4 4s$ $^2P_{3/2}$ transition. Tunable coherent VUV radiation was generated by four-wave difference frequency mixing in Kr using two dye lasers pumped by a XeCl excimer laser.

Results are graphically shown in Figure 1 with available literature data. Our results are in good agreement with the previous absolute rate studies, but lie systematically lower than the results from most previous relative rate investigations in 1-700 Torr. The simplest explanation for the scatter of the relative rate data, and the fact that the relative rate data generally are above the absolute rate data in Fig. 1, is that formation of OH radicals is a complication in relative rate studies conducted in the presence of oxygen. The previous relative rate studies were conducted either in air, or in air and N_2 diluents. Peroxy radicals will be formed during the chlorine atom initiated oxidation of isoprene and the reference compounds used in previous relative rate studies conducted in air. It has been shown recently that the reactions of peroxy radicals with HO_2 radicals can generate OH radicals. The formation of OH radicals will lead to an overestimation of k(Cl+isoprene) in relative rate experiments conducted in air. For the purposes of representing the chemistry of isoprene in atmospheric models we recommend a pressure independent value of k(Cl+isoprene) = (3.44 ± 0.32) × 10^{-10} cm^3 molecule^{-1} s^{-1} based upon the present work.

References

[1] G. P. Brasseur, J. J. Orlando, G. S. Tyndall, Atmospheric Chemistry and Change, Oxford University Press, 1999.

[2] J.-H. Xing, K. Takahashi, M. D. Hurley, and T. J. Wallington, Kinetics of the reaction of chlorine atoms with isoprene (2-methyl 1,3-butadiene, $CH_2=C(CH_3)CH=CH_2$) at 297 ± 2 K, *Chem. Phys. Lett.*, 472, 39-43, 2009.
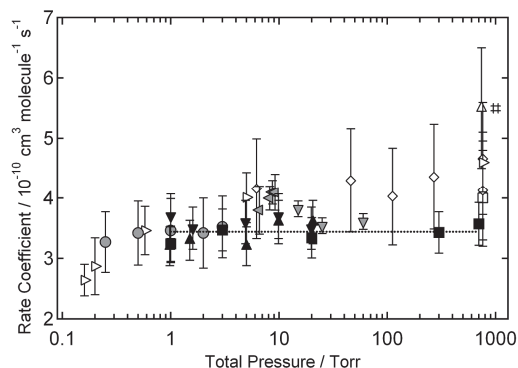
Figure 1 Rate coefficient k(Cl+isoprene) at 297±2K. Our data are shown in filled marks. The dotted line is the average value from our work at 1-700 Torr.

Simultaneous observation of vertical wind and hydrometeor fall velocity in stratiform precipitation by the Equatorial Atmosphere Radar and a polarization lidar

(Laboratory of Radar Atmospheric Science, RISH, Kyoto University)

Tomoaki Mega, Masayuki K. Yamamoto, Hiroyuki Hashiguchi, and Mamoru Yamamoto

Precipitation has two types; stratiform and convective. In the upper part of stratiform precipitation, ice particles grow up into snowflakes through depositional growth, riming growth, and aggregation. Latent heat released by deposition generates upward air motion, which supports a growth of large-sized snowflakes [1]. Therefore simultaneous measurement of vertical wind (W) and hydrometeors is a key for understanding processes in stratiform precipitation.

The Equatorial Atmosphere Radar (EAR) is a clear-air radar operated at 47-MHz frequency [2]. The EAR has an excellent capability of measuring echoes from clear-air turbulence and hydrometeors simultaneously. Linear deoplaization ration (LDR) measured by polarazation lidar is useful for knowing phase (ice, water, or mixed phase) and nonsphericity of hydrometeors. 1.3-GHz Doppler radar, which has higher sensitivity for hydrometeors than the EAR, was used to measure hydrometeor fall velocity (V_h). The experiment was done as "Cloud observation campaign using Lidar and Equatorial Atmosphere Radar (CLEAR)" carried out during December 2008.

Figure shows altitude profiles of W, hydrometeor fall velocity (V_h), lidar scattered power ($P_\parallel$) and LDR observed during the stratiform precipitation event on 8 December 2008. Owing to hydrometeor melting, V_h rapidly increased with decreasing altitude at 4.6-5.0 km (Figure b). W was upward (about 0.1 m s^{-1}) above 6.2 km and downward below 4.0 km due to latent heating and hydrometeor evaporation, respectively (Figure a). LDR increase in the altitude range 4.8-7.0 km with decreasing altitude suggests an increase of the degree of nonsphericity caused by aggregation (Figure d). These results indicate that simultaneous observation by the EAR and polarization lidar is useful for comprehensive understanding of the processes in stratiform precipitation region.

References

[1] Houze, R. A., "Nimbostratus", *Cloud dynamics*, Academic Press, pp. 196-220, 1993.

[2] Fukao, S., H. Hashiguchi, M. Yamamoto, T. Tsuda, T. Nakamura, M. K. Yamamoto, T. Sato, M. Hagio, and Y Yabugaki, "Equatorial Atmosphere Radar (EAR): System description and first Results", *Radio Sci.*, vol. 38, no. 3, 1053, doi:10.1029/2002RS002767, 2003.
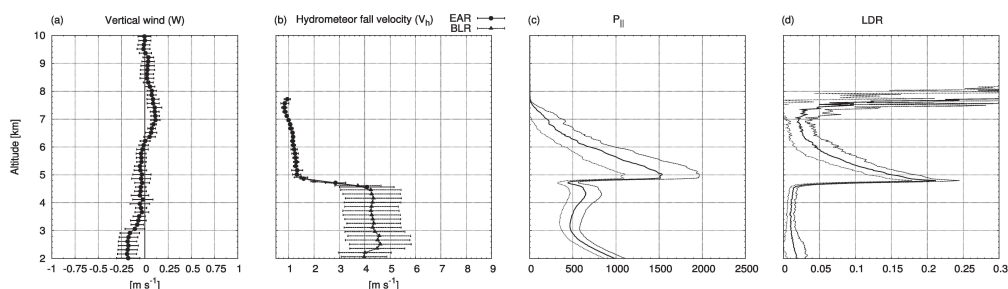
Figure. Altitude profiles of (a) W, (b) V_h, (c) $P_\parallel$, and (d) LDR. Error bars in (a) and (b) and thin curves in (c) and (d) show standard deviation.

Chitin nanofibers from marine bio-resources

(Laboratory of Active Bio-based Materials, RISH, Kyoto University)

Md. Iftekhar Shams, Hiroyuki Yano

Chitins are the main components in crab and shrimp shells, in the outer skins or cuticles of other arthropods, and in the molluscan shells of squid, and they are chemically identical to cellulose except that the secondary hydroxyl group on the carbon atom of the cellulose molecule is replaced by an acetoamide group. Chitin in the crustacean shells have the alpha type crystal structure where all molecular chains are arranged in an anti-parallel mode with strong intermolecular hydrogen bonding. The microfibers form layers producing a plywood-like structure. The microfibers recognize each other and arrange themselves in an orderly fashion. The crystalline microfibers contain nanofibrils, approximately 300 nm long and 2-5 nm wide. In this study, we have demonstrated the successful fabrication of chitin nanofibers having a uniform width of 20-30 nm from crab shells using simple mechanical process.

The starting material was dried crab shell flake of *Paralithodes camtschaticus* (Red king crab) sieved through 30-60 mesh. To extract nanofibers efficiently, chitin can be isolated from the cuticle by a series of decalcification and deproteinization steps using acid and alkali treatments, respectively. The wet chitin was suspended in water at 1% concentration and subjected to the high speed blender for 10 min at a rotating speed of 37000 rpm and kept at never dried condition. Despite its water-swollen condition, chitin exhibited a wide-ranging distribution of fiber widths. Thus, we added acetic acid to the pure chitin slurry, adjusted the pH value to 3-4, and then placed the mixture in a high-speed blender for 10 minutes. Surprisingly, a colloidal structure was obtained, indicating that the chitin-fiber slurry was homogeneously dispersed in water. SEM image (Fig.1) reveals that well-constructed chitin nanofibers were fabricated by controlling pH value and simple blending technique. These nanofibers have an average width of about 20-30 nm.
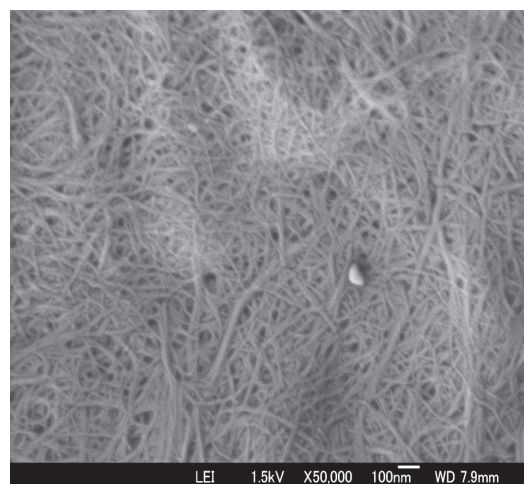

Figure 1. chitin nanofibers extracted from crab shells via high-speed blender under acidic conditions (pH 3-4)

An interesting observation was noticed during the filtration process to produce chitin nanofiber sheet. Possessing both hydroxyl and amine/*N*-acetyl functionalities, water suspension of chitin nanofibers was vacuum filtered 9 times faster compared to cellulose nanofibers to prepare nanofiber sheet. This is a prominent advantage of chitin nanofibers over cellulose nanofibers from the commercial viewpoint. Furthermore, the obtained nanofibers are small enough to retain the transparency of neat acrylic resin. At a visible wavelength of 600 nm; chitin/acrylic resin nanocomposite transmitted 87.3% of light, the fibrillated chitin fiber networks degraded only 3.2% light transmission of neat acrylic resin. Most interestingly, chitin nanofibers acrylic resin films exhibited much higher transparency compared to cellulose reinforced acrylic resin films despite the similar refractive indexes (RI) and width of both kinds of nanofibers. This high transparency of chitin composites may attribute to the close affinity between less hydrophilic chitin nanofibers and the hydrophobic resin. In addition, the incorporation of chitin nanofibers contributes the significant improvement of the thermal expansion and mechanical properties of the neat acrylic resin.

A foldable material with high light transmittance and low thermal expansion is a promising candidate for the substrate of continuous roll to roll process in the manufacturing of various optoelectronic devices such as flat panel displays, flexible displays and solar cells.

Aging of Wood - Elucidation of color changes as comparison between natural aging and accelerated aging -

(Laboratory of Sustainable Materials, RISH, Kyoto University)

Miyuki Matsuo, Misao Yokoyama, Kenji Umemura, Shuichi Kawai

The deterioration of wood as a material is due to biodegradation, weathering, and aging. In conditions under which biodegradation and weathering can be avoided by careful maintenance, the service life of wood can exceed a thousand years as proven by Horyuji temple, which is the oldest wooden building in the world. The elucidation of the wood aging mechanism is important not only for the preservation and restoration of wooden historical buildings but also for purposes of basic wood research.

Previous researches have observed that the changes of wood properties during natural aging seem similar to that during heat treatment under dry conditions. Based on the empirical data, they suggested that wood aging is a mild thermal oxidation at ambient temperature and can be accelerated by heat treatment. We aim to theoretically evaluate the mechanism of wood aging by kinetic analysis, to predict the changes of wood properties at room temperature, and to compare the predicted changes with the properties obtained from naturally aged wood.

Figure 1. Untreated specimen as control (a), colored specimens during natural aging for approx. 1600 years (b) and heated at 180°C for 12 hours (c).

While we have evaluated some properties of naturally aged wood samples from Japanese historical buildings [1], the color of wood is a typical index of the properties which sufficiently changes during natural aging and is measured in non-destructive process. We measured the color of naturally aged wood and heat-treated wood. Then, the data obtained were analyzed kinetically to determine whether they could be explained as the result of a mild thermal oxidation at ambient temperature. Sample preparations were as follows; samples corrected from Japanese historical buildings were cut into specimens; recently felled down hinoki (*Chamaecyparis obtusa* Endl.) wood were cut into samples, completely dried, and then heated at 90, 120, 150, 180°C for the durations ranging from 0.5 hour to approx. 2 years. Figure 1 shows some of specimens. Based on the successful kinetic analysis [2], we conclude that the color change of wood during natural aging is almost explained as thermal oxidation while somewhat accelerated possibly by the hydrolysis due to the moisture in air. Furthermore, the result allows to predict the color changes at any time and temperature. Compared with the predicted color changes, the internal color variation of recently felled wood was relatively small. This implies that the color changes accompanied with natural aging begin with tree harvesting and wood processing [3].

We are expanding these results to other wood properties and species which will lead a further understanding of the wood aging mechanism.

References

[1]Yokoyama, M., Gril, J., Matsuo, M., Yano, H., Sugiyama, J., Clair, B., Kubodera, S., Mitsutani, T., Sakamoto, M., Ozaki, H., Imamura, M., Kawai, S. "Mechanical characteristics of aged hinoki wood from Japanese historical buildings", *C. R. Phys.* 10(7) 601-611, 2009
[2]Matsuo, M., Yokoyama, M., Umemura, K., Gril, J., Yano, K., Kawai, S. "Color changes in wood during heating: Kinetic analysis by applying a time-temperature superposition method" *Appl. Phys. A* 99(1) 1-6, 2010
[3]Matsuo, M., Yokoyama, M., Umemura, K., Sugiyama, J., Kawai, S., Gril, J., Kubodera, S., Mitsutani, T., Ozaki, H., Sakamoto, M., Imamura, M. "Aging of wood - Analysis of color changes during natural aging and heat treatment -", *submitted to Holzforschung*
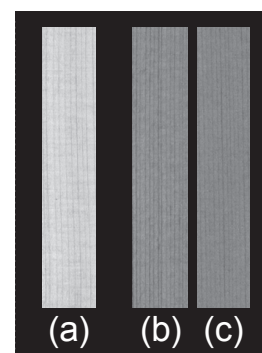
Investigation of Natural Frequency and Dumping Factor of Wooden Eco-House after Three Years since Completion

(Laboratory of Structural Function, RISH, Kyoto University)

Kohei Komatsu, Takuro Mori and Akihisa Kitamori

As an assigned research subject of 2009 RISH mission research projects, our project team investigated dynamic characteristics of so-called "Wooden Eco House", which was completed in September 2006 and has been used for about three years, using dynamic measuring methods. At first, very small level vibration of Eco House were measured (called as ambient vibration test). As the next step, in order to search the natural frequency of the house, the sweep harmonic excitation tests were carried out within the ranges of 0.1 to 15.0 Hz by synchronizing three portable shaking force generators which were fixed on the second story floor of Eco house as shown in Fig. 1.
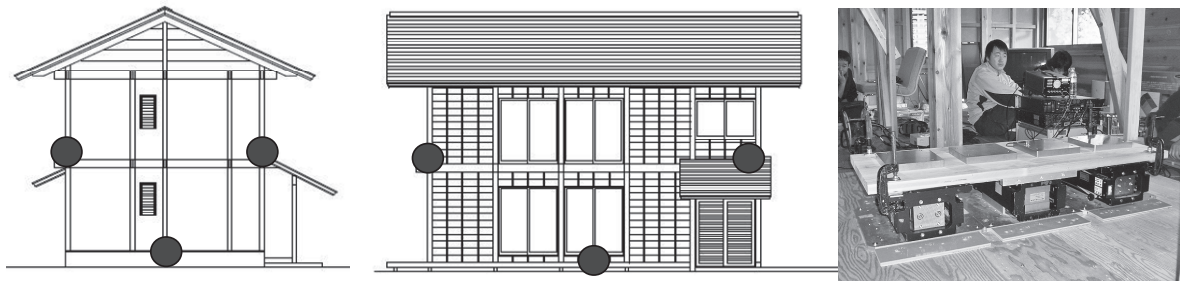

Figure 1. Locations of velocity meters and feature of excitation test on the second floor.

Figure 2 shows a power spectrum of velocity measured along span direction, from which we can see the first natural frequency at east face was 4.0Hz while the value at west wall face was 4.5Hz. The difference between both faces seems to be come from that of specification of shear walls. After the sweep harmonic excitation tests, in order to estimate the dumping factor of the house, free vibration tests were done by applying forced vibration under the natural frequency of 3.9 Hz for span direction then gave sudden cut off of the power from the three shaking force generators. Figure 3 shows a free vibration record of east face from which we could estimate the dumping factor to be about 5% for span direction.
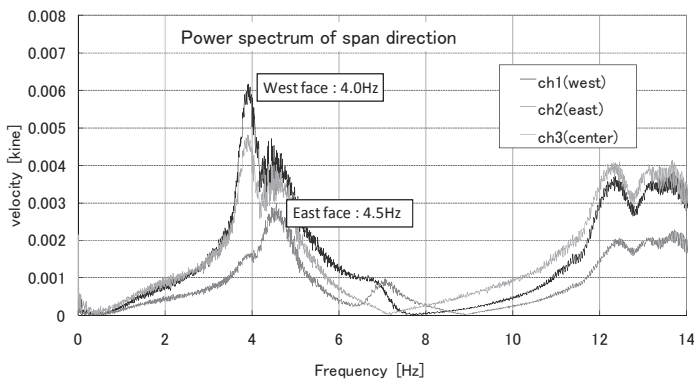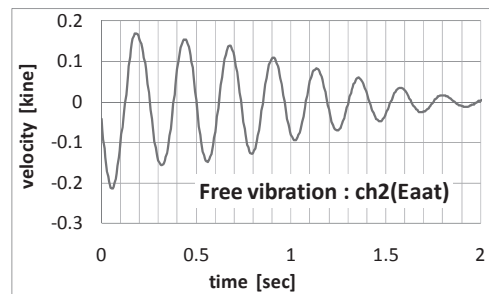

Figure 2. Power spectrum of span direction.

Figure 3. Free vibration wave record.

Acknowledgements

Evaluation of biodiversity of termites and wood-decaying fungi in tropical plantation forests

(Laboratory of Innovative Humano-Habitability, RISH, Kyoto University)

Tsuyoshi Yoshimura

Tropical forests contain the highest biodiversity in the world. Conserving biodiversity is crucial to maintain ecosystem services, which benefit human well-being. But tropical rain forests are still decreasing for many purposes; cutting for timber, oil-palm plantation, *Acacia* plantation for pulp production, shifting cultivation, *etc*. These changes in land-use caused habitat loss and even extinction of many organisms. The most important threats to mono-cultural plantation forests are disease and pests caused by other organisms, such as microorganisms and insects. In natural forests, the threats are likely to be secured by biological diversity. Therefore, the biodiversity of the plantation forests must be key information to evaluate the sustainability of the forest management. The strongest impact on decreasing ecosystem services in tropical rain forest is habitat loss. Maintaining biodiversity requires adequate landscape structure or management procedure. Our objective is to clarify termite and wood-decaying fungi diversity in plantation and conservation forests with different disturbance intensity. Termites and wood-decaying fungi are most important organisms that can convert lignocelluloses into low-molecular substrates, and are known to be good indicators of the forest soundness. We would like to clarify faunal and floral differences along with tree ages and distance from conservation forest as a species source to discuss what plantation should be to maintain ecosystem services.

The survey sites and protocols are as follows:

Borneo Island: *Acacia* Hybrid mono-cultural plantation forests and conservation forests near Keningau, Sabah, Malaysia.

Vietnam: *Acacia* Hybrid mono-cultural plantation forests in Tan Lap and conservation forests at Cat Tien National Park.

For the termite survey, the standardized protocol of a belt-transect method is applied. A 2 m x 100 m belt-transect is divided into 40 sub-transects (1 m x 5 m), and the one sub-transect is surveyed for termite fauna by a single people for 30 min (Fig. 1). All termite samples are kept in EtOH and brought back to Japan for identification. Four 4 m x 60 m belt-transects perpendicular to the 100 m termite belt-transect are subjected to the quantitative survey of wood-deteriorating fungi. A 60 m x 100 m arena is also surveyed for the total faunal assemblage. All fruiting bodies of wood-decaying fungi from the belt-transect and the arena are collected and dried, and brought back to Japan to be identified.

Figure 1. The belt-ransect termite survey in Cat Tien National Part, Vietnam.

Results obtained for the last two years show that termite fauna and wood-deteriorating fungal flora are strongly affected by mono-cultural plantation. Comparing the termite fauna among the sites, the age of plantation does not have significant positive effect on species richness, whereas the termite biomass is increased with the age. The plantation sites and the conservation sites have completely different fungal flora, and it is estimated that 20-30 years are not long enough to recover the original fungal flora in the plantation sites.

Computer Simulations of Wave-Particle Simulations in Space Plasmas

(Laboratory of Computer Simulation for Humanospheric Sciences, RISH, Kyoto University)

Yoshiharu Omura

We have clarified a long-standing issue on the generation process of whistler-mode chorus emissions in the Earth's magnetosphere by performing computer simulations based on particle models [1]. We develop a nonlinear wave growth theory of VLF chorus emissions [2], taking into account the spatial inhomogeneity of the static magnetic field and the plasma density variation along the magnetic field line. We derive theoretical expressions for the nonlinear growth rate and the amplitude threshold for the generation of self-sustaining chorus emissions. We assume that nonlinear growth of a whistler mode wave is initiated at the magnetic equator where the linear growth rate maximizes. Self-sustaining emissions become possible when the wave propagates away from the equator during which process the increasing gradients of the static magnetic field and electron density provide the conditions for nonlinear growth [3]. The amplitude threshold is tested against both observational data and self-consistent particle simulations of the chorus emissions. The self-sustaining mechanism can result in a rising tone emission covering the frequency range below the equatorial electron gyrofrequency.

The same nonlinear mechanism works for electromagnetic ion cyclotron (EMIC) waves with left-handed polarization. We recently found an observation of discrete rising tone emissions emerging from EMIC waves with a constant frequency. We have named them as EMIC triggered emissions [4], and reported its theoretical analysis [5], extending the theory developed for whistler-mode chorus emissions.
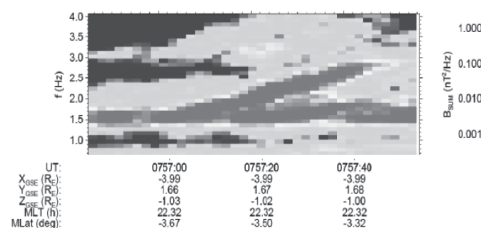

Figure 1. Dynamic spectrum of Pc1 waves observed by Cluster spacecraft.

References

[1] Hikishima, H., S. Yagitani, Y. Omura, and I. Nagano, Full particle simulation of whistler-mode rising chorus emissions in the magnetosphere, *J. Geophys. Res.*, 114, A01203, doi:10.1029/2008JA013625, 2009.

[2] Y. Omura, Y. Katoh, and D. Summers, Theory and simulation of the generation of whistler-mode chorus, J. Geophys. Res., 113, A04223, doi:10.1029/2007JA012622, 2008.

[3] Y. Omura, M. Hikishima, Y. Katoh, D. Summers, and S. Yagitani, Nonlinear mechanisms of lower-band and upper-band VLF chorus emissions in the magnetosphere, *J. Geophys. Res.*, 114, A07217, doi:10.1029/2009JA014206, 2009.

[4] J. S. Pickett, B. Grison, Y. Omura, M. J. Engebretson, I. Dandouras, A. Masson, M. L. Adrian, O. Santolik, P. M. E. Decreau, N. Cornilleau-Wehrlin, and D. Constantinescu, Cluster observations of EMIC triggered emissions in association with Pc1 waves near Earth's plasmapause, *Geophysical Research Letters*, 37, L09104, doi:10.1029/2010GL042648, 2010.

[5] Y. Omura, J. S. Pickett, B. Grison, O. Santolik, I. Dandouras, M. Engebretson, P. M. E. Decreau, A. Masson, Theory and Observation of Electromagnetic Ion Cyclotron Triggered Emissions in the Magnetosphere, *J. Geophys. Res.*, in press, 2010.

Application of Microwave Power Transmission

(Laboratory of Applied Radio Science for Sustainable Humanosphere , RISH, Kyoto University)

Naoki Shinohara and Tomohiko Mitani

Our laboratory started in April 2010 after retirement of Prof. Kozo Hashimoto. In our laboratory, there are three main research topics as follows;

· Research of Space Solar Power Station/Satellite (SPS)
· Research of Microwave Power Transmission (MPT) for Various Applications
· Research of Advanced Microwave Processing for Biomass Refinery and Creation of New Materials

In FY2009, RISH got governmental budget for the research of the SPS, MPT and microwave processing. One is new anechoic chamber with clean room and high power microwave absorbers for experiments of the SPS and MPT, Another is high efficient phased array with GaN amplifiers and MMIC phase shifters for the SPS and MPT. These are under developing (2010). New microwave processing equipments and measurement system of bio materials were introduced in the end of FY2009. The research of advanced microwave processing was elected for 'Flagship collaborative research' in the RISH. We will advance the microwave processing research with the new research equipment.

Research Activities for the SPS

In Japan, 'Basic plan for space policy' was established by Strategic Headquarters for Space Policy in June 2009. This Basic Plan for Space Policy forged this time is based on the Basic Space Law established in May 2008 and is a Japan's first basic policy relating to space activities. In the plan, the SPS was selected on major nine systems. The above research equipments of the anechoic chamber and phased array will be used for the R&D of the Japanese SPS with all Japan researchers. Prof. Shinohara is a chairperson of the METI's SPS R&D committee which collaborates with JAXA. We discuss the short range roadmap to experimental MPT satellite and the long range roadmap to the SPS.

Collaborative Researches of the MPT applications

In FY2009, we have some collaborative researches of the various MPT applications. One is the wireless charging system for an electric vehicle with 2.45GHz. In FY2009, we realized beam collection efficiency of 76% between the transmitting slot antenna and rectenna array. The other is short distance MPT system with 24GHz for FWA (Fixed Wireless Access), which is used for telecommunications network whose interconnections between nodes are implemented without the use of wires. We developed the first 24GHz rectenna with approximately 40% conversion efficiency.

Microwave Pretreatment System for Bioethanol Production from Woody Biomass

We developed prototypes of a continuous-flow-type microwave pretreatment system for bioethanol production from woody biomass. Efficient pretreatment process prior to enzymatic saccharification process is essential for profitable bioethanol production from woody biomass. Microwave pretreatment is expected as an efficient and energy-cost-saving method to enhance enzymatic susceptibility. The objective of the present study is to develop an efficient, high-volume, and continuous microwave pretreatment system toward commercially-based bioethanol production. Prototype experiments and quantitative estimation of energy balance were also conducted. This work is supported by the New Energy and Industrial Technology Development Organization (NEDO) project, "Development of Technology for High-efficiency Conversion of Biomass and Other Energy", whose leader is Prof. Takashi Watanabe of the RISH.

Novel Space Environment Monitor, Instrument, and Space Mission Concepts

(Laboratory of Space Systems and Astronautics, RISH, Kyoto University)

Hiroshi Yamakawa, Hirotsugu Kojima, and Yoshikatsu Ueda

Near-Earth Asteroid Flyby Survey Mission Using Solar Sail

A novel near Earth (NEA) asteroid flyby survey scheme is proposed using solar sailing technology by reducing the orbital angular velocity of the solar sail and keeping the heliocentric distance constant. This realizes the potential for a very fast NEA survey mission of about one year from the time of launch, and could enhance the asteroid discovery rate. This scheme also has the potential for indirectly reducing the potential Earth impact risk by accumulating information about asteroids, as well as directly reducing this risk by utilizing the spacecraft as a kinetic impactor.

Lorentz Force Spacecraft Formation Dynamics

We proposed a spacecraft formation scheme augmented by Lorentz force using the interaction between an electro-statically charged satellite and the Earth's magnetic field to provide a thrust. The orbital dynamics is investigated and the existence of periodic orbits is shown which can be applied for near-future formation flight missions.

Magneto-Plasma Sail (MPS) Space Propulsion System

An MPS (Magneto-Plasma Sail) is a unique propulsion system, which travels through interplanetary space by capturing the energy of the solar wind, which inflates a weak original magnetic field made by a super-conducting coil of about 2-10 m in diameter with an assistance of a high-density plasma jet. From our theoretical estimations, momentum transfer from the solar wind to a spacecraft with a coil is large enough if the plasma source is operated to inflate only the magnetic field away from the spacecraft. Our activities in 2006 are as follows: (a) Sizing (mass, dimension, current, etc.) of the super-conducting coil to produce magnetic field around the spacecraft, (b) Preparation of the experiment facility to measure magnetic field, temperature, current etc. around super-conducting coil.

Monitor system for Space Electromagnetic Environments (MSEE)

The main objective of the MSEE (Monitor system for Space Electromagnetic Environments) is to monitor the electromagnetic disturbances caused by human activities in space. It consists of the small sensor units distributed around the target space.   Our main activities on the development of the MSEE in 2006 are as follows: (a) Development of the analogue ASIC containing the differential amplifiers and A/D converters, (b) Simulation study on the location estimation method for each sensor unit.

Wave-Particle Interaction Analyzer(WPIA) Instrument for Spacecraft Observation.

For a practical application of a plasma wave instrument, a direct measurement system of wave-particle interactions is one of the important systems to the space science mission. WPIA instrument can observe wave-particle interactions by calculation of the cross correlation functions between obtained waveforms and detected particles onboard. Our designed system is assembled in one FPGA (Field Programmable Gate Array) IC and data calibration and correlation method is programmed in FPGA.

Electrical and Thermal Properties of Carbonized Wood Based Composites

(Graduate School of Agriculture, Laboratory of Innovative Humano-habitability, RISH, Kyoto University)

Joko Sulistyo

Considerably interest has developed in the use of wood-based carbon material as new source of carbon for engineering applications [1]. Carbonized wood has been widely utilized for many applications, from adsorbents [2], to carbide ceramics for thermoelectric materials [3] and high temperature filters [4], etc. These variety applications of carbonized wood-based composites are influenced by the pores and microstructure in carbonized wood. The control of pores and microstructure in carbonized wood through heat treatments conditions such as temperature, heating rate and reaction time, may lead to new applications of the material. The microstructure and pores in carbonized wood in this study were exploited to the development of carbonized wood-based composites for thermal management in space solar power satellite (SPS). This application needs thermal conductive materials exhibiting high thermal conductivity with anisotropic behavior. The thermal conductive materials were tried to be developed by alternates layering of carbonized wood and graphite in three-layer laminated composite or by generating silicon carbide-carbon (SiC/C) composites from reaction of carbonized wood with turbostratic structure with SiO_2.
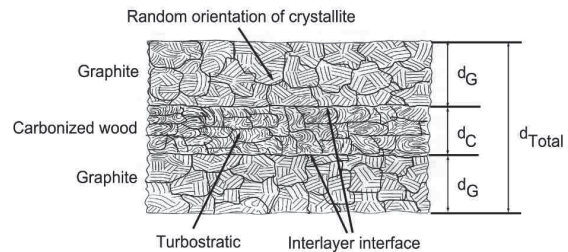

Figure 1. Schematic structure of three-layer laminated C/G composites for thermal conductive material with a function to discharge the heat from two sides

In first part of study, microstructure arrangement and pore structure development in carbonized biomass during heat treatment at 700 ºC with slow or fast heat treatment were investigated. Oil palm shell heat treated at 300 ºC followed by slow heat treatments at 700 ºC with a heating rate of 10 ºC/min created opened micropores with a broad size distribution together with ordering microstructure of carbon. Fast heat treatments at same temperature with heating rates from 75 to 2000 ºC/min produced microstructure with a narrow pore size distribution of 0.1-0.28 nm at the maximum distribution due to cracks generated during heat treatment [5] which appeared as structural disordering. Slow and fast heat treatments produced dissimilar micropore distributions. Oil palm shell heat treated at 300 ºC and then at 600 ºC influenced on less structural arrangement of microstructure and micropore development during slow or fast heat treatments. The heat treatment at 700 ºC was necessary to develop micropore and microstructure in carbonized biomass which is crucial in the development of thermal conductive materials.

Table 1. Thermal conductivity of C/G composites, single layer of graphite and carbonized wood

Sample name	Structure (Layers)	Measured (W/m K)		
		k_H	k_V	H/V ratio
G100	1	33.30	8.81	3.78
C/G=5/95	3	18.93	3.45	5.49
C/G=10/90	3	19.85	1.95	10.17
C/G=20/80	3	13.25	1.58	8.40
C/G=33/67	3	8.86	1.20	7.41
C/G=60/40	3	5.66	0.81	7.02
C/G=70/30	3	5.23	0.80	6.55
C/G=80/20	3	3.53	0.61	5.80
C100	1	1.14	0.50	2.31

k_H, thermal conductivity in the horizontal direction; k_V, that of in the vertical direction; *H/V ratio*, ratio of thermal conductivity between in the horizontal and in the vertical directions; SL-G, single layer composite, of graphite; SL-C, that of carbonized

In 2nd part, composites with anisotropic thermal behavior for thermal conductive material in SPS were developed by alternating layers of laminated graphite and carbonized wood (C/G composite), as shown in

Fig. 1, which were prepared by heat treatment at 700 ºC. The effect of the weight fraction of carbonized wood, particle size and interlayer interface on the thermal conductivity and the ratio of thermal conductivity in the horizontal and vertical directions (H/V ratio) to the plain surface of samples were discussed. Alternate layers of graphite and carbonized wood improved the anisotropic thermal conductivity of C/G composites. Thermal conductivity was good within graphite layers due to the high order microstructure and poor perpendicular to the graphite layers due to the presence of a layer of carbonized wood consisted of turbostratic microstructure and micropores [6]. The weight fraction of carbonized wood affected the thermal conductivity and the H/V ratio. The highest H/V ratio was obtained at 10 wt% of carbonized wood particles with a size of 25-32 μm. Particle size and interlayer interface were found to affect the anisotropic thermal conductivity. Alternately layered composites of two-phase components, such as graphite and carbonized wood, may be useful in thermal management applications in SPS. Improved thermal conductivity is necessary in order to obtain an effective thermal conductive material.

In 3rd part, a high electrical and thermal conductivities SiC/C composite as alternative surface layer in a three-layer laminated thermal conductive material was developed from carbonized wood. SiC composite was potential due to exhibiting good thermal conductivity, high strength, heat-resistance and low density and being produced not at very high temperature [4]. The electrical and thermal conductivities were investigated in relationship with the microstructure and growth of β-SiC crystal and carbon crystallite in SiC/C composite which was maintained by a solid-solid reaction between SiO_2 and carbonized wood or a gas-solid reaction between SiO and carbonized wood. The highest electrical and thermal conductivities of 1.17 x 104 $\Omega^{-1}m^{-1}$ and 25 w/m.K were obtained in SiC/C composite prepared by a solid-solid reaction followed by sintering at 1800 ºC, due to the largest amount of β-SiC, the highest degree of ordering of the carbon microstructure and the smallest amount of SiO_2. The thermal conductivity could be improved to 101 W/m.K by increasing the density of the composite from 1.2 to 1.82 g/cm^3. In the case of SiC/C composite prepared by a gas-solid reaction, SiO gas infiltrated carbonized wood to form β-SiC which may suppress the growth of carbon crystallite resulted in the low thermal conductivity of 1.6 w/m.K, due to the less growth and the less ordering the microstructure of β-SiC crystal and carbon crystallite in the composite. Such high thermal conductivity SiC/C composites are preferable for alternative face in three-layer laminated thermal conductive material for an effective thermal management in SPS. The low thermal conductivity of the composites, can be used for an alternative core layer. A three-layer laminated composite of SiC/C with markedly different thermal conductivity of 101 W/m.k on the surface layers and 1.6 W/m.K on the core at a thickness ratio of 50/50 was predicted to exhibit anisotropy behavior with the calculated H/V ratio of 15.9 and the thermal conductivity in the horizontal and vertical directions of 51.2 and 3.2 W/m.K, respectively.

References

[1] Byrne, C.E., D.C. Nagle, "Carbonization of wood for advanced materials applications", *Carbon*, vol. 35, pp. 259-266, 1997.
[2] Pulido, L.L., T. Hata, Y. Imamura, S. Ishihara, T. Kajimoto, "Removal of mercury and other metals by carbonized wood powder from aqueous solution of their salts", *J. Wood Sci.*, vol. 44, pp. 237-243, 1998.
[3] Fujisawa, M., T. Hata, H. Kitagawa, P. Bronsveld, Y. Suzuki, K. Hasezaki, Y. Noda, Y. Imamura, "Thermoelectric properties of porous SiC/C composites", *Renewable Energy*, vol. 33, pp. 309-313, 2008.
[4] Greil, P., "Biomorphous ceramics from lignocellulosic", *J. Eur. Ceram. Soc.*, vol. 21, pp. 105-118, 2001.
[5] Kercher, A.K., D.C. Nagle, "Microstructural evolution during charcoal carbonization by X-ray diffraction analysis", *Carbon*, vol. 41, pp. 15-27, 2003.
[6] Sulistyo, J., T. Hata, M. Fujisawa, K. Hashimoto, Y. Imamura, T. Kawasaki, "Anisotropic thermal conductivity of three-layer laminated carbon-graphite composites from carbonized wood", *J. Mater Sci.*, vol. 44, pp. 734-744, 2009.

Preparation of Artificially Degraded Wood Samples Similar to Archaeological Waterlogged Wood.

(Laboratory of Innovative Humano-habitability, RISH, Kyoto Universiy, Present: Nara National Research Institute for Cultural Properties)

Yohsei Kohdzuma

Some effective conservation methods for archaeological waterlogged wooden objects have been developed. However, the choice of the procedure or the extent of the treatment still is made by experience because it is difficult to obtain the detailed characteristics of waterlogged woods without destruction. If we can obtain large amounts of uniformly degraded samples, we could expect to establish a systematic procedure for waterlogged wood conservation. Because it is difficult to obtain such samples from "real" waterlogged woods, it is important to prepare an artificially degraded specimen, which is similar to the actual waterlogged wood in physical, chemical and microstructural aspects.

In order to investigate degradation process of buried archaeological wooden objects, core samples of soil, underground water and wood samples obtained from several points of Aoya-Kamijichi archaeological site were analyzed. From the results of underground water analyses, oxidation-reduction potential (ORP), dissolved oxygen (DO) and concentration of ions varied periodically through a year. ORP of soils even from the neighboring boring points were different. The soil layers that included wooden archaeological objects were subacidity and oxidative. However, as the ORP of underground water varied periodically through a year, that of the soil layers also may vary in the same manner. The woods in upper and sand layer were decayed severely. In the silt layer of high water content which oxygen is not supplied sufficiently, it is considered that woods were decayed anaerobicaly.

To understand the degradation degree of waterlogged woods, we related the physical and mechanical properties, and the chemical compositions with one another. Generally, it is known that in the initial stage of degradation, hemicelluloses prefecturally is attacked, and in this study it was proved that cellulose and lignin also are degraded considerably in further stages of degradation. An approximate linear relationship, obtained by the maximum moisture method, was observed between the reciprocals of basic specific gravities and the maximum moisture contents, although the changes in the densities of wood substances should be considered. The shrinkage resulted from collapse is increased over 300% of maximum moisture content(Figure 1). The irreversible shrinkages in the tangential directions increased with decreases of the basic specific gravities. The compressive strength parallel to grains was closely with the specific gravities.

To prepare artificially models of waterlogged wood, we degraded woods by acid, Fenton's reagent, brown-rot fungi, and soft-rot fungi, and their physical properties were compared with those of waterlogged woods reported in the previous paper. Some of the physical properties of the degraded woods: decreases in basic specific gravities, compressive strength, and hardness, and increases in shrinkages and maximum
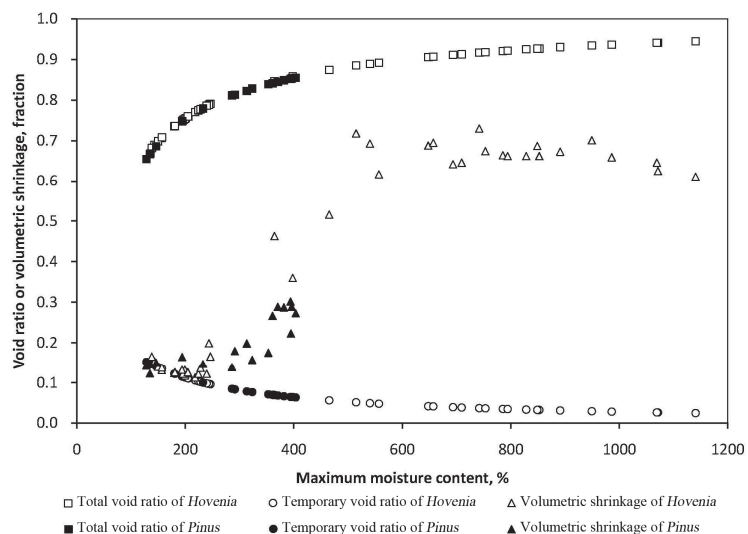

Figure 1. Changes of void ratio and volumetric shrinkage of archaeological waterlogged wood.

moisture contents, were similar to those for waterlogged woods. The basic specific gravity, shrinkage in the tangential direction, and maximum moisture content of the wood degraded by brown-rot fungi resulted in 0.132 g/cm^3, 25.6%, and 700%, respectively, the values being similar to those of the most deteriorated waterlogged wood. A linear relationship between the maximum moisture content and the reciprocal number of the basic specific gravity was observed in all artificially
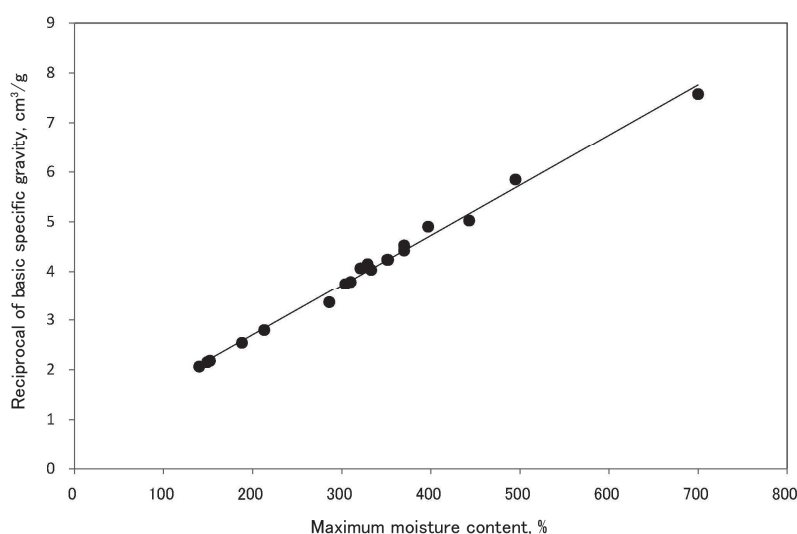

Figure 2. Relationship between maximum moisture content and reciprocal of basic specific gravity.

degraded samples, and the relationship also was applied to the waterlogged wood(Figure 2). However, it was impossible to attain the desired degradation level by the fungi treatment because the decay progressed unevenly within the specimen. Considerably polysaccharides were lost during both acid and fungi treatments similarly to waterlogged wood, but lignin probably was subjected to considerable chemical change by the former treatment.

In the wood samples artificially degraded with Fenton's reagent, the basic specific gravity decreased to 0.171 g/cm^3, while the maximum moisture content and the shrinkage in the tangential direction increased to 495% and 16.2 %, respectively. These values were comparable to those of moderately degraded waterlogged softwood. Similar to the waterlogged wood, the density of wood substance degraded with Fenton's reagent decreased with the progress of degradation. A good relationship was found between the treated/control ratio of shrinkage and the reciprocal number of the basic specific gravity. Within the experiment, considerable lignin, as well as polysaccharides, was lost by the Fenton's reagent treatment. This tendency was similar to that of the waterlogged wood, although the degree of degradation was different. From the analysis of the neutral sugar composition of the wood treated with Fenton's reagent, it was found that cellulose was degraded to the same degree as hemicelluloses, as is the case of real waterlogged wood.

PEG impregnation method, vacuum freeze drying and alcohol xylene resin method were applied to artificially degraded woods which had similar physical properties to archaeological waterlogged wood. When wood samples degraded by acid hydrolysis and wood rot fungi were treated by vacuum freeze drying and alcohol xylene method respectively, the contents of PEG and dammar resin were different depending on the degradation treatment even in the same degradation degree.

It is cleared that absorbance of solute to wood substance should be considered from polarity and interaction of solvent with temporary void in evaluation of efficiency of conservation method.

It is difficult to apply the artificially degraded wood to consideration of conservation treatment of extremely degraded archaeological wood. It is possible to apply the artificially degraded wood to consideration of diffusion, penetration and absorbance of agent.

Comparative Characterization of Bistrifluron as a Novel Slow-Acting Termiticide

(Laboratory of Innovative Humano-Habitability, RISH, Kyoto University, Present: Environmental Health Division, Sumitomo Chemical Co., Ltd)

Shunichi Kubota

Rhinotermitid subterranean termites of two genera, *Coptotermes* and *Reticulitermes* are serious damaging pests of structures all over the world. All termite species have their well-organized eusocial caste systems, which discriminate those from other pest insects in terms of management methods. Therefore, methods for controlling entire colonies using bait system had been exploited and various slow-acting insecticides had been tested as bait toxicants for years. Since a benzoylphenylurea (BPU) compound, hexaflumuron was found to be effective for colony elimination of subterranean termites in 1990's, various bait products containing BPUs have been commercialized. Although BPUs are so far only chemicals that can successfully eliminate termite colonies of *Coptotermes* and *Reticulitermes* when they are used as bait toxicants, a new BPU bisrifluron has not yet been studied in details so far.

Termiticidal efficacy of bistrifluron as a bait toxicant against Japanese subterranean termites, *Coptotermes formosanus* and *Reticuliterme speratus*

The insecticidal efficacy of bistrifluron as a bait toxicant against the Japanese subterranean termite species, *Coptotermes formosanus* Shiraki and *Reticulitermes speratus* (Kolbe) was evaluated in the laboratory. The no-choice feeding tests using filter-paper bait and paper-towel bait were conducted with *C. formosanus* and *R. speratus*, respectively. Slow-acting insecticidal efficacy was seen in *C. formosanus* workers upon exposure to 5,000 and 50,000 ppm bistrifluron bait, while there was no significant increase in mortality at 500 ppm in the 8-week test. Faster insecticidal efficacy was observed with *R. speratus* workers upon exposure to 5,000 and 50,000 ppm bistrifluron bait. Unlike *C. formosanus*, the two colonies of *R. speratus* showed different responses at 500 ppm bistrifluron, which might suggest dose-dependent feature of bistrifluron.

Termiticidal efficacies of fenobucarb and permethrin against Japanese subterranean termites, *Coptotermes formosanus* and *Reticulitermes speratus*

The insecticides fenobucarb and permethrin were examined in the laboratory with regard to their termiticidal efficacy and speed of action against *C. formosanus* and *R.speratus*. Test insects were first exposed to filter paper treated with given concentrations of each insecticide for 21 days (continuous exposure) or two .hours (short-term exposure), and changes in termite mortality were compared. The termite species had no significant effect on the termiticidal efficacy or speed of action of the two insecticides. Both fenobucarb and permethrin exhibited very fast actions. The former showed a delayed action only in the 21-day exposure test, whereas the latter did not exhibit any delayed action even in the 21-day exposure test.

Response of *Coptotermes formosanus* to soil sreated with Baktop[®] MC, microencapsulated fenobucarb

The chemical barrier effect of microencapsulated fenobucarb against *C.formosanus* was examined in the laboratory. Fenobucarb had a significantly faster lethal effect when applied orally than dermally to worker termites. Soil that had been treated with ≥ 50 ppm (wt/wt) microencapsulated fenobucarb had a barrier effect within a single day, and could stop or retard the penetration of termites for 7 days. Microencapsulated fenobucarb did not act as a repellent agent. The results mean that microencapsulated fenobucarb is a fast-acting contact-poisonous termiticide with a good barrier effect as a soil-treatment agent. These features are favorable for preventive termiticide but not for bait toxicant.

Detailed evaluation of bistrifluron as a bait toxicant against *Coptotermes formosanus*

Bistrifluron was evaluated with regard to its efficacy against workers of *C. formosanus* using three laboratory tests. In the no-choice feeding test, the mortality of bistrifluron-treated worker termites was

significantly higher than that of termites exposed to the same concentrations of hexaflumuron [*e.g.*, 6 week at 500 ppm (wt/wt), 4 week at 5,000 ppm (wt/wt) and 2 week at 50,000 ppm(wt/wt)] and untreated controls. Bistrifluron showed higher dose-dependence and a faster speed of action than hexaflumuron. Both bistrifluron and hexaflumuron had feeding-deterrent effects at 5,000 ppm in the two-choice feeding test, although the mortality of worker termites exposed to bistrifluron or hexaflumuron at 5,000 ppm was not significantly different from untreated controls. In the allogrooming inhibition test, allogrooming behavior of termites and termite movement was affected at one week before termites died when exposed to 5,000 ppm bistrifluron. These results indicate bistrifluron to be effective as a bait toxicant at 5,000 ppm, while bistrifluron may cause some feeding repellency at ≥5,000 ppm.

Lethal dosage and horizontal transfer of bistrifluron among worker termites of *Coptotermes formosanus*

The lethal dose and horizontal transmission of bistrifluron was examined against workers of *C. formosanus* in the no-choice feeding test. When the termite workers were exposed to 5,000 ppm (wt/wt) bistrifluron bait for one week, toxicity appeared slowly with an LT_{50} (50% lethal time) 6.2 weeks. Much faster efficacy was observed after a two-week exposure, which gave an LT_{50} 3.1 weeks. The amount of bistrifluron recovered from moribund termites was 397.7 ± 57.66 ng/termite at 5 weeks in the one-week exposure, while 492.0 ± 50.09 ng/termite was recovered at three weeks in the two-week exposure. Bistrifluron was analyzed quantitatively from the head, legs, alimentary tract and other parts of the termite body, and the amounts were 90.5, 4.5, 60.8 and 559.1 ng/termite, respectively, immediately after the one-week exposure to 5,000 ppm bistrifluron bait. The rate of bistrifluron transferred from 20 donors to 20 recipients for one week was 6% of that taken by the donors during the one-week exposure to 5,000 ppm bistrifluron bait, and much smaller amounts of bistrifluron were transferred afterward from donors to recipients. The amount of bistrifluron that was originally ingested by *C. formosanus* workers, appeared to partly remain in the termite body (approximately 400 ng/termite).

Uptake of b by foraging workers of *Coptotermes formosanus*

Uptake of bistrifluron by foraging workers of *C formosanus* at three sites in the arena; workers on baits were collected and analyzed for bistrifluron content aliquid chromatography. All foragers disappeared from the one site with a bistrifluron bait about two months after the bait placement, while a few foragers were present at the two sites with an untreated bait. Termites contained more bistrifluron if collected from the site with a treated bait than with an untreated bait (~1026 vs. ≤196 ng of bistrifluron/termite). About one month after treated and untreated bait sites were switched, foragers returned to the site with bistrifluron bait, and the colony was shortly eliminated thereafter. Lethal quantities of bistrifluron (483-1380 ng/termite) were present in most of workers before the colony was eliminated.

It can be concluded by the series of experiments: 1) bistrifluron acts on termites extremely slowly in comparison to termiticides used as soil termiticides; however, 2) its efficacy is significantly dose-dependent and appears relatively faster in comparison to hexaflumuron; 3) bistrifluron inhibits colony-maintaining activities of termites like allogrooming behavior before the colony is eliminated; 4) a lethal dose of bistrifluron against *C. formosanus* is ≥400 ng per termite; 5) some portion of bistrifluron once taken up by foraging termites would remain in termite body for weeks, while the rest of bistrifluron is discharged; 6) sufficient amount of bistrifluron can be taken up by foraging termites owing to its slow action and subsequently bistrifluron would be transferred among most of foragers, and 7) Feeding deterrency of bistrifluron as a reflection of its dose-dependence is not always an unfavorable characteristics since the improvement of feeding preference by termites could lead to faster colony elimination. These conclusions clearly support that bistrifluron is a potential candidate as a bait toxicant.

Analysis of Natural Materials and Structures by Non-Contact Strain Measurements Methods

(Graduate School of Agriculture, Laboratory of Structural Function, RISH, Kyoto University)

Hassel Beatriz Ivón

Abstract

Non-contact strain measuring methods were applied to the study of mechanical properties of wood and mud materials. Focusing on the shear properties, from the macrostructure (millimeters, at the annual growth scale), to their application in timber structures.

The shear testing device, called single cube apparatus [1,2,3] (SCA) provides with a large central area of near-to-pure shear strains (Figure 1). It was used in combination with digital speckle photography (DSP) to study the transverse shear modulus (G_{RT}) of Norway spruce (*Picea abies*). Thus, a micromechanical model based on geometrical hexagonal cells[4,5], relating the density gradient to the G_{RT} was developed. It was found a strong dependence of G_{RT} to the relative density (Figure 2). This makes the average G_{RT} of spruce lower than other softwood species of similar average density and different density gradient[6]. Moreover, digital image analysis was use to obtain the elastic mechanical properties of natural and compressed Japanese cedar (*Cryptomeria japonica* D. Don). These properties were included in a finite elements model (FEM) of a wooden-bricks shear wall. It was designed as an interlocking system, which takes advantage of the properties of compressed softwood[7]. The stiffness of the wall was successfully increased by adding prismatic compressed elements, recovering their radial dimension due to springback properties.

Mud material, main component of traditional Japanese walls[8,9], presents several difficulties for testing, due to their high porosity and brittleness. Digital strain measurements were introduced in combination with digital image correlation, as an adequate method for obtaining the material properties. DSP was directly applied to the analysis of prefabricated mud shear wall units (PMWU). Extensive scrutiny on their performance relative to the number of connectors linking the PMWU to the external timber frame was carried out. Furthermore, a FEM including the detailed characteristics of the composition of the PMWU's was created. The model produced results that agreed accurately with the experimental outcomes.

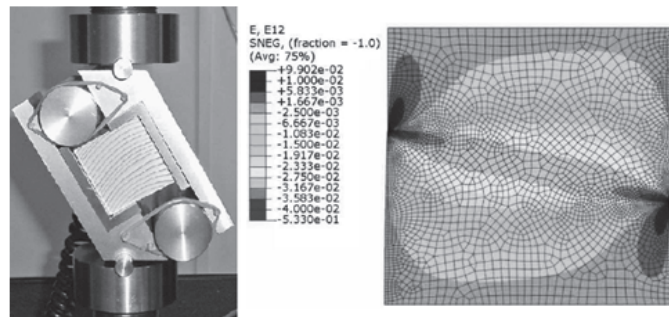Non-contact strain measuring methods allowed to accurately obtaining the basic properties of wood and mud

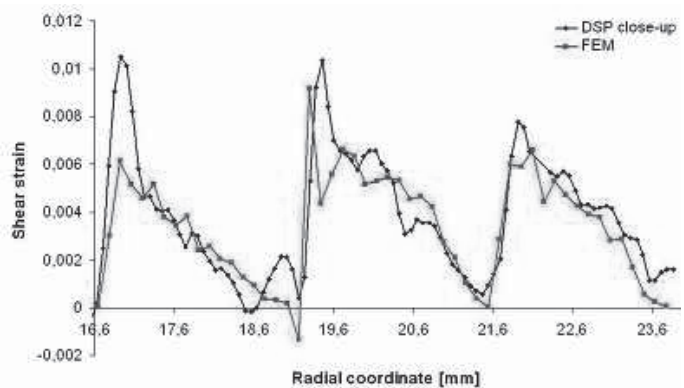Figure 1. Right: Single cube apparatus. Left: In-plane shear strain field, FEA results.

Figure 2. Shear strain profiles. Experimental DSP shear strain measurements and predicted shear strain using finite element analysis.

materials. Porosity and heterogeneity at the mm-scale were successfully avoided. It also helped improving the understanding of failure mechanism of softwoods due to annual ring effects. Furthermore, digital image analysis was directly applied to strain measurements of timber and mud shear walls. And FEM including the obtained properties are a powerful tool for predicting the behavior of such structures.

References

[1] Berard P, Yang P, Yamauchi H, Umemura K, Kawai S. Modeling of cylindrical LVL: Finite elements models of a flat interlocked LVL and a comparison of standard and non standard testing methods in the elastic domain. In: Proceedings of the *2nd international symposium on veneer processing and products*. Editor: Dai C. Vancouver, British Columbia, Canada; pp 428–435, 2006.

[2] Hassel I, Berard P, Komatsu K. Development of wooden block shear wall – Improvement of stiffness by utilizing elements of densified wood. *Holzforschung*; 62: 584-590, 2008.

[3] Hassel I, Berard P, Modén CS, Berglund LA. The single cube apparatus for shear testing - full-field strain data and finite element analysis of wood in transverse shear. Composites Science and Technology; 69: 877-882, 2009.

[4] Modén CS, Berglund LA. Elastic deformation mechanisms of softwoods in radial tension - Cell wall bending or stretching? Holzforschung; 62: 562-568, 2008a.

[5] Modén CS, Berglund LA. A two-phase annual ring model of transverse anisotropy in softwoods. Composite Science and Technology; 68: 3020–3026, 2008b.

[6] Shipsa A, Berglund LA. Shear coupling effects on stress and strain distributions in wood subjected to transverse compression. Composites Science and Technology; 67: 1362–1369, 2007.

[7] Kitamori, A. *Doctoral Thesis, Kyoto University, Japan, Department of Agriculture*, 2009. (In Japanese)

[8] Nakao M, Ichimonji R, Yamazaki Y, Ishibashi Y. An experimental study on shear resisting mechanism and shear strength evaluation method of mud-plastered walls. *Journal of Structural and Construction Engineering, Architectural Institute of Japan* (AIJ); 598: 109-116, 2005.

[9] Nakao M, Yamazaki Y. An experimental study on mud-plastered walls for evaluating ultimate strength and ductility. Part 8. Static incremental analysis by RBSM. *Architectural Institute of Japan*; 241-242, 2006. (In Japanese)

Reconstitution of cellulose synthesizing activity *in vitro* with algal and bacterial model

(Graduate School of Agriculture, Laboratory of Biomass Morphogenesis and Information, RISH, Kyoto University)

Akira Hashimoto

Extracting cellulose-synthesizing activity is well known to be very difficult because cellulose synthase is highly complex machinery of membrane protein complex. Until now, few model organisms have successfully provided *in vitro* cellulose synthesizing activity after extraction from cell membrane. This study aims to newly establish *in vitro* system to synthesize cellulose I microfibril. Two models are selected: *Micrasterias crux-melitensis* (a green algae) and *Gluconacetobacter xylinus* (a gram-negative bacterium). The former is unicellular and taxonomically categorized Zygnematale, which is considered to be the direct ancestor of land plants. Therefore it is likely a good model for studying cellulose biosynthesis in plants. The latter is a famous model that has been reported already, but the product is cellulose II of a non-native form. Then improving conditions was conducted for the purpose of synthesizing cellulose I microfibril *in vitro* by using this bacterial model.

Experiments

M. crux-melitensis was grown in *Volvox* medium. *G. xylinus* was grown in SH-medium including 0.1% celluclast (commercial cellulase, Novozyme Inc.). Cells were harvested and disrupted by French Press at 20,000 psi. Microsome prepared by differential centrifugation was solubilized by detergent to extract cellulose synthesizing activity. UDP-glucose (substrate) was added to this detergent-extract for *in vitro* synthesis of cellulose; c-diGMP (cyclic-diguanyl monophosphate, allosteric effector of cellulose synthase in *G. xylinus*) was included together when *G. xylinus* was used. The synthesized product was examined by TEM (Transmission Electron Microscopy) and IR (InfraRed) spectroscopy. c-diGMP was enzymatically synthesized by recombinant DGC (diguanyl cyclase) protein [1].

Results

When *M. crux-melitensis* was used, two types of fibers were observed by TEM: short and long fibers (Figure 1A). The former was more frequently observed than the latter, and looks like those reported as callose [2]. The latter was likely cellulose microfibril when judged by appearance. Actually IR spectra suggested that the product might be a mixture of callose and cellulose. Further examination is in progress.

For *G. xylinus*, two nonionic detergents (*n*-decyl-β-D-maltoside (DM) and *n*-dodecyl-β-D-maltoside (DDM)) were newly tried for solubilzing cell membrane. Electron micrographs by negative staining showed that the product is not microfibril but aggregation in which about 40 nm of particles get together (Figure 1B). Electron diffraction and IR spectra indicated that the product is cellulose II as well.

Acknowledgements

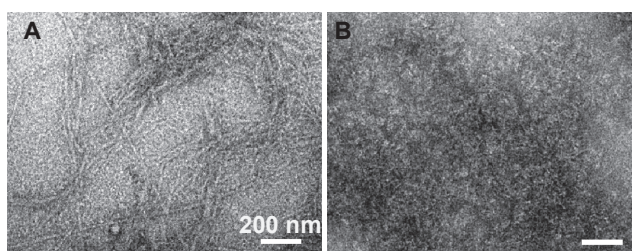The author appreciates Prof. Kazufumi Yazaki (RISH, Kyoto University) for the use of ultracentrifugation.

Figure 1. Electron micrographs (negative staining) of the *in vitro* product by *M. crux-melitensis* (A; digitonin used as detergent) and *G. xylinus* (B; DDM used).

References

[1] Tsukasa Ichikawa "Enzymatic synthesis of c-di-GMP by recombinant protein" *Sustainable Humanosphere*, no.6, in this issue (2010)

[2] for example, Joséphine Lai-Kee-Him, Henri Chanzy, Martin Müller, Jean-Luc Putaux, Tomoya Imai, Vincent Bulone. "*In vitro* versus *in vivo* cellulose microfibrils from plant primary wall synthases: structural differences" *J. Biol. Chem.* vol. 277, no.40, pp 36931-36939, 2002.

Dynamic bending properties of natural fibers measured by electrostatic vibration system

(Graduate School of Agriculture,
Laboratory of Biomass Morphogenesis and Information, RISH, Kyoto University)

Toshiyuki Iburi

A system to measure dynamic properties of a single plant fiber is developed. The fiber is placed in an oscillating electrostatic field and the resonance frequency, damping of vibration both in vacuum and in air are successfully measured. With this new instrument, physical properties of traditional native fibers, namely, *Boehmeria nivea, Boehmeria sylvestris, Laportea macrostachya* was investigated.

Experiments

Natural fiber samples were collected from field in the late June, 2008. The phloem fibers (bast fibers) was peeled off from the plants and purified by pectinase treatment. They were washed thoroughly and then freeze dried. The experimental setup developed in the laboratory is shown in Figure 1[1]. Conditions for measurement are as follows: frequency region 20Hz～6000Hz、distance between electrodes 0.2～0.5mm, oscillating voltage 100V+-70V. Young's modulus of a single fiber is calculated from the equation $E=4f^2\pi^2(l/1.875)^4\rho A/I$, where f: resonance frequency l: length of a fiber ρ: density A: cross sectional area I: geometrical moment of inertia.

Results

Averaged Young's moduli of fibers from *B. nivea, B. sylvestris,* and *L. macrostachya* were calculated to be 83.8GPa, 66.1GPa, and 90.9GPa, respectively. Interestingly, the modulus from *L. macrostachya* was statistically smaller than those of the other two species. The technique developed in this study may be applied for identifying the origin of natural fiber, which is often required in archeological science.

Acknowledgement

I would like to thank Dr Tomohiko Mitani, RISH Kyoto University, for developing experimental setup, and Dr Rie Endo, the same institute, for valuable suggestions on traditional natural fibers.

References

[1] Meredith, R, Hsu, B-S: "Dynamic bending properties of fibers: Effect of temperature on nylon 66, terylene, orlon, and viscose rayon" J. Polym. Sci. 61, pp. 271-291, 1962
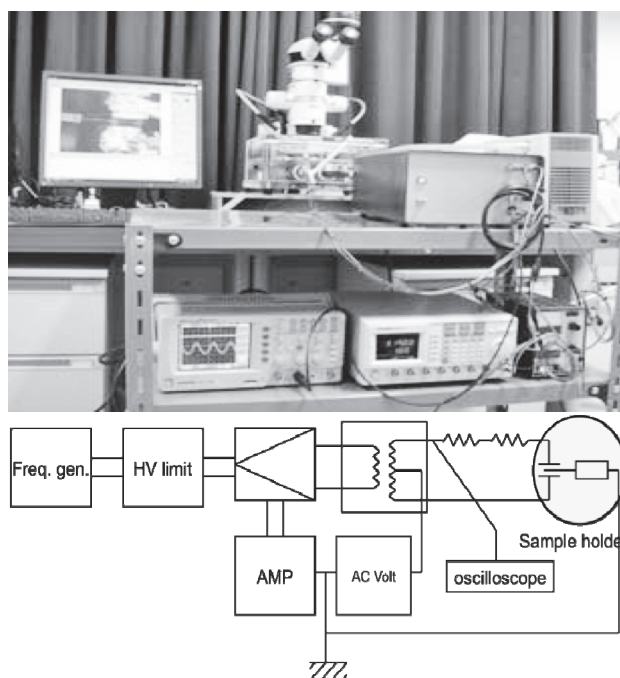
Figure 1 A general experimental setup.

Enzymatic synthesis of c-di-GMP by recombinant protein

(Graduate School of Agriculture, Laboratory of Biomass Morphogenesis and Information, RISH, Kyoto University)

Tsukasa Ichikawa

Cellulose biosynthesis is one of the important biological activities, which has been maintained by many living organisms for more than hundred millions years on the earth. Cellulose synthase is known to be membrane protein complex, which is clearly difficult to study. A cellulose-producing bacterium *Gluconacetobacter xylinus* is chosen as an experimental model in this study because it is a prokaryotic single-cell organism, which makes experimental design simpler. In this bacterium, c-diGMP (cyclic-diguanyl monophosphate) plays an important role in cellulose biosyntheis as an allosteric effector. This study aims to establish the enzymatic synthesis of c-diGMP.

Experiments

Enzyme that synthesizes c-diGMP is known as DGC (diguanyl cyclase) or "GGDEF" protein. First, VCA0956 from *Vibrio cholerae*, which was previously shown to have DGC activity *in vitro* [1], was selected and its genomic DNA was inquired to ATCC (American Type Culture Colllection). However, the DNA of this pathogenic bacterium was not available. Then a homologue was found by blastp search: DGC from *Shewanella oneidensis* MR-1 (hereafter called as SoDGC). The *sodgc* gene was amplified by PCR and inserted into pBAD vector (Invitrogene Inc., US) for expression by *E. coli*. Recombinant DGC expressed with hexahistidine-tag fused was purified by IMAC (Immobilized Metal Affinity Chromatography), and mixed with GTP to convert it to c-diGMP. The resultant c-diGMP was finally purified by anion-exchange chromatography with mobile phase of the gradient of ammonium carbonate, as previously described [2].

Results

Recombinant DGC protein expressed by *E. coli* was successfully purified as confirmed by SDS-PAGE (Figure 1). Processing of the c-di-GMP synthesis reaction by anion-exchange chromatography gives two peaks of elution at 1.6% and 3.2% ammonium carbonate (Figure 2). By MALDI-ToF MS, it was indicated that the former and the latter contain GTP and c-diGMP, respectively. Successful synthesis of c-diGMP was further confirmed by LCMS-IT-TOF analysis: fragments obtained by MS/MS was consistent with the molecular formula
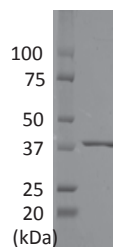

Figure 1 SDS-PAGE stained by Coomasie Brilliant Blue. Lane 1: marker, Lane 2: recombinant DGC purified by IMAC.

Figure 2. Elution profile of the resultant c-diGMP synthesis reaction on anion-exchange chromatography with ammonium carbonate gradient.

Acknowledgements

The author appreciates Prof. Takashi Watanabe, Drs. Koichi Yoshioka and Hiroshi Nishimura (RISH, Kyoto University) for mass spectroscopic analysis.

References

[1] Tamayo, R., Tischler, A. D., Camilli, A. "The EAL domain protein VieA is a cyclic diguanylate phosphodiesterase", *Journal of Biological Chemistry*, vol. 280, no. 39, pp 33324-33330, 2005.

[2] Ross, P., Aloni, Y., Weinhouse, C. "An unusual guanyl oligonucleotide regulates cellulose synthesis in *Acetobacter xylinum*", *FEBS letters*, vol. 186, no. 2, pp 191-196, 1985.
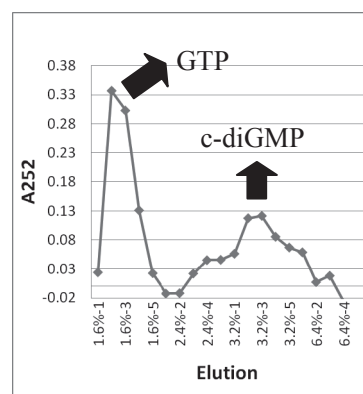
Exposure of polysaccharides in lignocellulosics with peroxy acids produced by enzymatic perhydrolysis

(Graduate School of Agriculture, Laboratory of Biomass Conversion , RISH, Kyoto University)

Makoto Abiru

In enzymatic saccharification of lignocellulosics, access of enzymes to exposed cellulose surfaces is an initial key step in triggering the hydrolysis. Peroxy acids are potential agents to degrade plant cell wall components to expose cellulose. In this study the author focused on enzymatic production of peroxy acids, and evaluated their reactivity to expose cellulose surfaces in lignocellulosic biomass. For the production of peroxy acids, perhydrolysis of fatty acids by lipase was applied. Exposure of the polysaccharide by peroxy acids was analyzed using green fluorescent protein (GFP)-labeled carbohydrate-binding modules (CBMs) from *Clostridium josui*. As a specific markers for crystalline and non-crystalline cellulose, *Cj*CBM3 and *Cj*CBM28 were used, respectively. Distribution of the exposed cellulose surfaces after reaction was analyzed using confocal laser scanning fluorescence microscope.

Japanese cedar wood was partially delignified by glycerolysis at 200°C for 6 min using microwave irradiator. Insoluble pulp fraction was separated, washed successively with acetone and water, and used for the analysis of the exposed cellulose. Peroxy acids were prepared by the reactions of lipase from *Penicillium camemberti* with octanoic acid and H_2O_2 in chloroform. *m*-Chloroperbenzoic acid (*m*CPBA) was used as a standard compound of peroxyacid.

The partially delignified pulp was treated with peroxyoctanoic acid, and adsorption of *Cj*CBM28-GFP and *Cj*CBM3-GFP on the substrate was analyzed before and after reaction. Adsorption of these probe molecule to crystalline and non-crystalline cellulose increased depending on the conditions for the pretreatment. Increase in the adsorption of fluorescent CBMs were also found in the treatments with *m*CPBA. Analysis with confocal laser fluorescence microscope showed that the lignocellulosics treated with peroxy acid was extensively fibered (Figure 1).

Peroxy acids formed by enzymatic perhydrolysis are the potential agent to expose cellulose surfaces in lignocellulosics. This expands roles of lipase and other lipid-related (per)hydrolytic enzymes from the degradation of lipids to the exposure of cellulose surfaces, thereby accelerating microbial and enzymatic degradation of lignified plant cell walls.
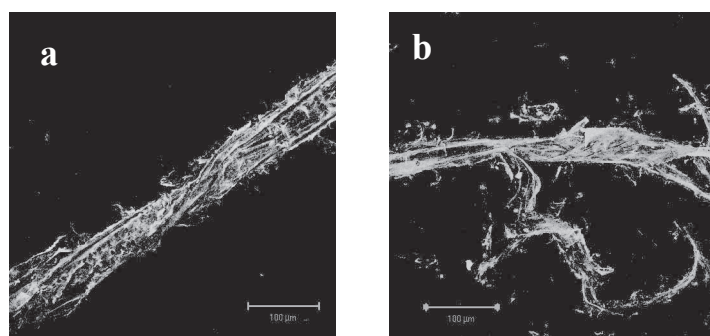
Figure 1 Confocal laser fluorescence microscopic photographs of partially delignified pulp from Japanese cedar wood after adsorption of *Cj*CBM28-GFP.
(a) untreated,　(b) treated with peroxyoctanoic acid

Screening of extracellular oxidized metabolites produced by selective white rot fungus

**(Graduate School of Agriculture,
Laboratory of Biomass Conversion , RISH, Kyoto University)**

Yuichi Setogawa

Ceriporiopsis subvermispora is known as one of the best selective lignin-degrading fungi. Due to the unique wood decay system degrading lignin without intensive damage of cellulose, extensive research on the applications of the fungus to biopulping, preparation of feed for ruminant animals and pretreatments for enzymatic saccharification and fermentation have been carried out. In selective white rot by *C. subvermispora*, lignin degradation proceeds without penetration of extracellular enzymes into the wood cell wall regions. This unique phenomenon indicates that low molecular mass metabolites are principally responsible for the lignin degradation because these metabolites are able to diffuse into the wood cell wall regions where extracellular enzymes cannot penetrate.

Thus far, manganese peroxidase (MnP)-mediated lipid peroxidation has been proposed as a ligninolytic system at an incipient stage of wood decay by *C. subvermispora.* Production profiles of MnP, saturated and unsaturated fatty acids and their oxidation products, hydroperoxides and TBARS supported that the fatty acids are produced by the fungus and oxidized during the early stage of wood decay. In addition to the production and oxidation of fatty acids, new secondary metabolites suppressing ion redox cycle have been found. Thus far, four novel alk(en)ylitaconic acids; tetradecylitaconic (ceriporic acid A), hexadecylitaconic (ceriporic acid B), (*Z*)-7-hexadecenylitaconic (ceriporic acid C) and (*E*)-7-hexadecenylitaconic acid (ceriporic acid D) have been isolated and identified from the cultures of *C. subvermispora*. It was demonstrated that the alkylitaconic acids suppressed reduction of ferric ions, thereby attenuating production of celluloytic hydroxyl radicals by the Fenton reaction system.

In the present study, the author focused on oxidized metabolites produced by *C. subvermispora.* The selective white rot fungus, *C. subvermispora* ATCC90467 was grown on a potato dextrose agar medium at 25°C for 5 days. The preculture was inoculated into 200 ml of SDW medium in 500-ml Erlenmeyer flask and incubated statically at 28 °C for 3 weeks. After incubation, the culture was gently filtered with nylon mesh. The residues of fungal hyphae on the nylon filter were filtered off using vacuum pump and the metabolite solution was collected. Then, ten times amount of ethanol was added to the solution to give white precipitates. After removing precipitates by centrifugation, the supernatants were purified by solid phase extraction, evaporated, and analyzed by LC-IT-TOF MS.

Screening of the metabolites by LC-IT-TOF MS revealed that this fungus produced a wide range of oxidized derivatives from long-chain alkyl and alkenyl carboxylic acids. Some of the oxidized derivatives were also found from wood meal cultures of the fungus. The oxidized metabolites are trait of the extracellular oxidative reactions in selective white rot, and important to understand the roles of secondary metabolites in the wood decay at a site far from enzymes.

Development of transformation and promoter assay system in selective lignin-degrading fungus, *Ceriporiopsis subvermispora*.

**(Graduate School of Agriculture,
Laboratory of Biomass Conversion, RISH, Kyoto University)**

Eiji Tanigawa

Introduction

Recently, wood biomass conversion systems have gained increasing attention as one of the solutions for the environmental problems, since cyclic utilization of wood is carbon-neutral. A white-rot fungus, *Ceriporiopsis subvermsipora* is able to degrade lignin selectively without intensive damage of cellulose. Thus, treatment of wood substrates by this fungus has been expected for a ecofriendly pretreatment in wood biomass conversion. To elucidate molecular mechanism for the selective lignin-degrading system by this fungus, it is essential to develop an efficient genetic transformation system. Furthermore, in basidiomycetes, promoter assay has been done using stable transformants, but they contained different copy numbers of exogenous reporter gene at various loci on the chromosome. So it is very difficult to evaluate accurate activity of a promoter in basidiomycetes. In this context, strongly desired is to develop a new promoter assay system which is completely unaffected by the insertion manner of the reporter construct in the chromosome.

Results and Discussion

In this work, a stable transformation system in *C. subvermispora* was developed for the first time, by modifying experimental conditions of the conventional PEG/CaCl$_2$ method in basidiomycetes. A number of drug resistant colonies were observed on the screening plate: a small portion of them maintained, despite the most remaining isolates (~95%) lost the drug resistance, during successive cultivations on the screening plate. The stable isolates were demonstrated as a integrated transformant in Southern hybridization analysis, whereas the unstable ones were decided to be a transient transformant and not a false positive, taking the fact that no drug resistant colonies were observed in no DNA control experiment. Next, we tried to evaluate activity of a series of promoter sequence which drives the drug resistant marker gene, by measuring the number of the transformants on the first screening plate. With this strategy, a deletion analysis of *C. subvermispora gpd* promoter was performed and, as a result, a 141-bp fragment was determined to be essential for the initiation of transcription. This result indicated that the system developed in this work is useful as a novel promoter assay system in basidiomycetes.

Filed Measurement of Water Vapor Distribution near Ground with a Small Raman LIDAR

(Graduate School of Informatics, Laboratory of Atmospheric Sensing and Diagnosis, RISH, Kyoto University)

Shuji Ohta

Water vapor is one of the most important atmospheric minor constituents, which significantly affects various meteorological phenomenon, such as precipitation, cloud formation, latent heat transport. Therefore, it is expected to develop a state-of-the-art measurement technique of water vapor distribution near such as volcanic fumarole and forest. The former is known as an indicator of volcanic activity. The latter leads to understanding forest-atmosphere interaction. Thus, measurement of water vapor distribution and variation at various fields is of great significance. A Raman lidar is an active remote sensing technique for profiling atmospheric parameters, including water vapor mixing ratio (WVMR). We have developed portable Raman lidars for profiling water vapor, and applied it for a field experiment at volcano and over forest.

First, we have improved performance of the lidar system by installing an electric shutter, and realized a laser control system with a laptop computer for automatic and continuous observation of WVMR at a remote field site.

Vertical and horizontal scanning observations around the volcanic crater at Mt. Aso were carried out on October 2008. The result clearly showed that there are two types of peak of WVMR with and without enhancement of BSR(Back Scatter Ratio). The former comes from fumarole clouds at a volcano, and the latter is cause by evaporation of volcanic lake. To our knowledge, this was the first measurement to distinguish two sorts of WVMRs sources at a volcano.

The observation over forest at Shigaraki was initiated in May 2009. Vertical cross section of water vapor distribution was observed for the night time, over the national forest. WVMR variations of an amplitude of 3.2 (g/kg) were detected, correlated with variations of aerosol backscatter ratio. And this indicates possibility of topographically-affected WVMR variations.

To summarize, we have developed a portable Raman lidar system for future applications, and successfully observed water vapor distribution near ground over a forest and a volcano.

Development of Range Imaging Wind Profiler for Observations of Atmospheric Boundary Layer

(Graduate School of Informatics, Laboratory of Radar Atmospheric Science, RISH, Kyoto University)

Yusuke Moritani

It is important to observe atmospheric turbulence in order to clarify developing processes of the atmospheric boundary layer. However, it is not so easy to observe atmospheric turbulence. In FY2003, the MU (middle and upper atmosphere) radar was equipped with an ultra-multi-channel system, which enabled us to observe three dimensional structures of the atmospheric turbulence by means of radar imaging techniques. Limitation of the MU radar is that it cannot observe the lower part of the atmosphere below 2 km, because it takes about 10 μs to switch from transmitting to receiving. Therefore we have developed a range imaging wind profiler for observing the atmospheric boundary layer by upgrading the 1.3-GHz wind profiler system (LQ7) installed at the Shigaraki MU Observatory (Figure 1).

Figure 1. LQ-7 wind profiler installed at the Shigaraki MU Observatory.

Frequency Domain Interferometry (FDI) is a technique to obtain high range resolution using the phase difference among receiving signals for various transmitting frequencies. We applied the FDI technique to LQ7 which was upgraded to use five frequencies of -500 kHz, -250 kHz, 0, +250 kHz, +500 kHz relative to 1357.5 MHz. As shown in Figure 2, FDI observation results using Capon method could provide us the detailed turbulence structure. Owing to severe ground clutter, the original data from the radar were not useful for the FDI analysis. We developed a technique to suppress the ground clutter, and succeeded in the FDI analysis. We have evaluated range imaging performance of LQ7 comparing with the observation results with other frequency radars. Vertical velocity and horizontal wind with LQ7 are consistent with those by other radars. Maximum observation height, which is defined by signal to noise ratio > -10 dB, is about 3.5 km in summer and about 2.5 km in winter. Developing process of the atmospheric boundary layer is observed with LQ7, which is impossible by the MU radar. Simultaneous observations with LQ7 and 35-GHz radar on September 24 and 25, 2009 show that the atmospheric boundary layer corresponds to cloud variations. Horizontal wind is consistent to the pressure distribution and topography. With their results, we concluded that the radar imaging technique applied to the 1.3-GHz wind profiler is very useful to study the lower atmosphere dynamics.
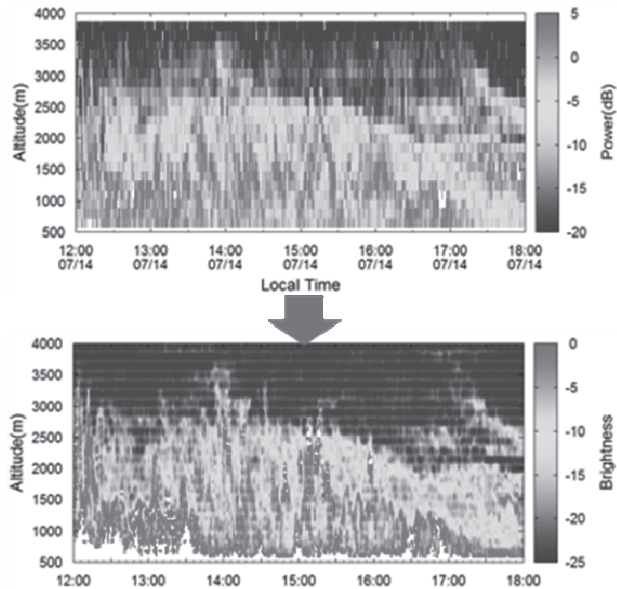

Figure 2. Example of time-height sections of echo intensities observed with standard mode (upper) and FDI mode (lower) of LO-7.

Nano-fibrillation of wood pulp using a high-speed blender

(Laboratory of Active Bio-based Materials, RISH, Kyoto University)

Kojiro Uetani

Cellulose microfibril bundles is known to be obtained as cellulose nanofibers (CNF) with diameters of 15-20 nm by mechanical fibrillation.[1] CNF having prospective mechanical properties such as high Young's modulus, high strength and very low coefficient of thermal expansion is expected to be utilized as a filler of next-gen nanocomposites.[2] We developed a novel and convenient preparation method to obtain CNF from wood pulp using a high-speed blender.

Experiment

The 30-60 mesh never-dried pulp, which α-cellulose content was 72.5 wt% and Klason lignin content was 0.1 wt%, was prepared by the WISE method of a cyclic treatment 10 times with a sodium chlorite (NaClO$_2$) solution under acidic condition (PH 4-5) at 80 ℃ for one hour. The suspensions of pulp fibers were agitated using a high-speed blender at different concentrations of pulp. As a reference, the suspension at a fiber content of 0.7 wt% passed one time through the grinder at 1500 rpm.

Result and discussion

The degree of fibrillation was evaluated indirectly by the transparency of their sheets after resin impregnation. The blender could fibrillate pulp to the same degree by the grinding method and the mechanical damage of fibers evaluated by XRD seems to be lesser. This agitating fibrillation method has several advantages allowing not only the control of the degree of fibrillation of pulp but also the observation of how the pulps are disintegrated into totally uniform nanofibers. The observation of the treatment process revealed that the straw-like pulp is fibrillated through a very characteristic way, by forming many "balloon like structures" as shown in Fig. 1. These balloons swelled more than twice as the original straw pulp and disintegrated to CNF in burst.

The fibrillation with changing parameters in agitation indicates that the optimum condition of fibrillation is pulp concentration of 0.7 wt % at 37000 rpm (see Fig.2). At each concentration, the agitating speed affects the degree of fibrillation. The faster speed makes pulp fibrillate faster. On the other hand, the degree of fibrillation proportionally increases up to the pulp concentration of 0.7 wt%, then decreases above 1.1 wt%. The degree or speed of fibrillation is affected by the pulp concentration.
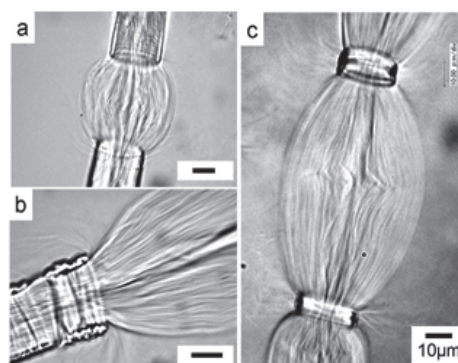

Figure 1. Digital micrographs of balloons occurring in the pulp fiber agitated at the concentration of 0.7 wt% with 37000 rpm.
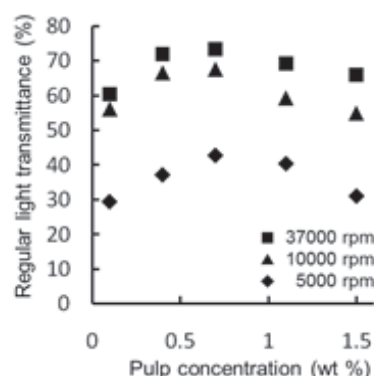

Figure 2. The regular light transmittance at 600 nm of 15 composites made of acrylic resin and 10 min agitated pulp at various agitating speed for pulp suspension of 0.1, 0.4, 0.7, 1.1 and 1.5 wt%.

References

[1] Abe, K.; Iwamoto, S.; Yano, H. *Biomacromolecules*, vol.8, pp.3276-3278, 2007.

[2] Berglund, L. A.; In *Natural Fibers, Biopolymers and Their Biocomposites*; Mohanty, A. K., Misra, M., Drzal, L. T., Eds.; *CRC Press Boca Raton*, FL, pp.807-832, 2005.

Surface chemical modification of cellulose nanofiber (octanoylation)

(Laboratory of Active Bio-based Materials, RISH, Kyoto University)

Naoki Yoshida

Surface chemical modification has potentials for broadening application of cellulose nanofibers (CNF). For chemical modification, it is necessary to exchange solvent dispersing CNFs from water to polar aprotic solvent. In this case CNFs have not to be aggregated and water has to be removed completely. Conventional solvent exchange method (by centrifugation or freeze-dry) is not enough to attain these requirements. In the study reported here, the author developed new solvent exchange method for surface chemical modification of CNFs. By the method, CNFs were octanoylated to yield CNF derivatives with hydrophobic surface, and some octanoylated CNFs were dispersed in hexane.

Materials and methods

1) New solvent exchange method

CNFs were prepared from the wood flour of cryptomeria using a grinder (MKCA6-3, Masuko Sangyo Co., Ltd.). A mixture of 0.82 wt% CNF aqueous slurry 12.20 g (CNF's dry weight : 100 mg) and N-methylpyrrolidone (NMP) 60 mL was agitated well and heated at 150 ℃ under atmospheric pressure for 2 h until water was almost evaporated. In order to remove slightly remaining water, the CNF-NMP slurry was heated at 150 ℃ under reduced pressure (100 hPa) until about 10 mL NMP was collected. Thus, 0.2 % CNF-NMP slurry was prepared without water.

2) Octanoylation

After pyridine was added into 0.2 % CNF-NMP slurry, octanoyl chloride was added slowly and then the mixture was heated at 60 ℃ for 6 h. After the reaction mixture was poured onto ethanol, octanoylated CNF precipitated were washed with ethanol thoroughly by using vacuum-filtration.

The structure of octanoylated CNFs were confirmed by ATR-IR spectra and the degree of substitution (DS) was determined by back titration. Then, octanoylated CNFs were subjected to wide angle X-ray diffraction, SEM observation and solvent dispersibility test.

Results and discussion

Octanoylation of CNFs were confirmed by IR spectra and the author found that surface chemical modification of CNF efficiently proceeded by using new solvent exchange method. And, chemical modification proceeded on only the surface of CNFs in the less than DS 0.55 and into the inside of crystal in the more than DS 0.87 according to wide angle X-ray diffraction and SEM observation. Figure 2 shows dispersibility of octanoylated CNFs in water and hexane. According to an increase in the DS, CNFs weren't dispersed in water, whereas CNFs were dispersed in hexane. Thus, there is difference in solvent dispersibility by DS.
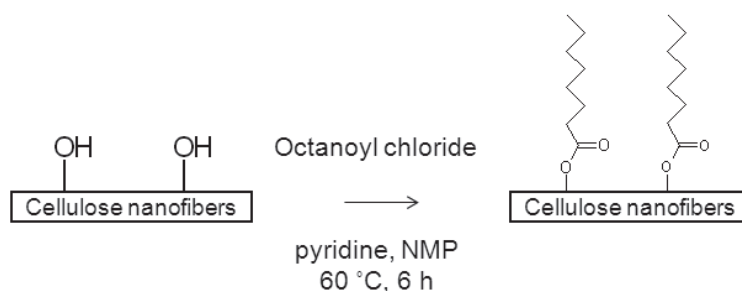

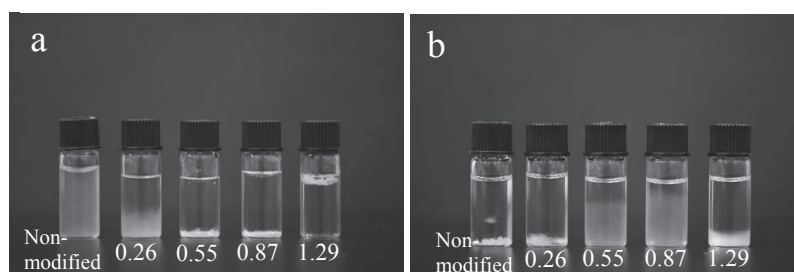Figure1. Octanoylation of cellulose nanofiber

Figure 2. Dispersibilty of octanoylated CNF in water (a) and hexane (b).
Figures are the degree of substitution (DS).

Preparation and property of surface deacetylated chitin nanofiber

(Graduate School of Agriculture,
Laboratory of Active Bio-based Materials, RISH, Kyoto University)

Takeshi Oku

Chitin in the crustacean shells such as crabs and prawns exists in the form of crystalline chitin microfibril of about 2-5 nm in width. Recently, it has been reported that the chitin nanofiber can be isolated by mechanical treatment under acidic condition. This is because cationization of amino groups on the surface of chitin microfibril promotes nanofibrilation. The chitin nanofiber is expected as a reinforcement to give optically transparent and the low thermal expansion composites. As chitosan, that is deacetylated chitin, has antimicrobial property, the surface deacetylated chitin nanofiber is expected to exhibit antimicrobial property. The present study clarified the property of the surface deacetylated chitin nanofiber.

Materials and methods

α-chitin from crab shell (Nacalai Tesque) was purified with 4wt% NaOH solution. The purified chitin was deacetylated with 20-40wt% NaOH solution at 90℃ for six hours under the stirring, and the obtained sample was analyzed by the ATR-IR and X-ray diffraction. The deacetylated chitin was dispersed in water at 1 wt %, and acetic acid was added to adjust the pH value to 3-4 to facilitate fibrillation. The slurry of 1 wt % deacetylated chitin was passed once through a grinder (MKCA6-3; Masuko Sangyo Co., Ltd.) at 1500 rpm. The obtained nanofiber was observed by FE-SEM (JSM-6700F; JEOL). The deacetylated chitin nanofiber slurries were converted to thin sheet by suction filtration, and dried at 110℃. The mechanical properties of the obtained thin sheets were evaluated by tensile test.

Results and discussion

Table.1 shows degree of deacetylation of the chitin prepared by NaOH solution at 90℃ for six hours. When the chtin was treated with 40wt% NaOH, α-chitin crystal structure changed, indicating that deacetylation occurred inside of α-chitin crystal. However, when 20-35wt% NaOH was used, the α-chitin crystal structure and crystal size did not change. These results demonstrate that deacetylation by 20-35wt% NaOH mostly takes place on the surfaces of α-chitin crystal.

The nanofibers obtained from untreated chitin were found to have a width of about 10-50 nm. On the other hand, the nanofibers obtained from 35wt% NaOH treated chitin demonstrated a uniform width of about 10 nm.

Figure.1 shows the results of tensile test. Young's modulus and tensile strength of sheet increased with the degree of deacetylation. Since the number of amino groups on the surface of chitin nanofibers increased due to deacetylation, it is suggested that the number of hydrogen bonds between nanofibers increased.

Table.1 Degree of deacetylation (DDA) of the chitin prepared with different NaOH concentration at 90℃ for six hours.

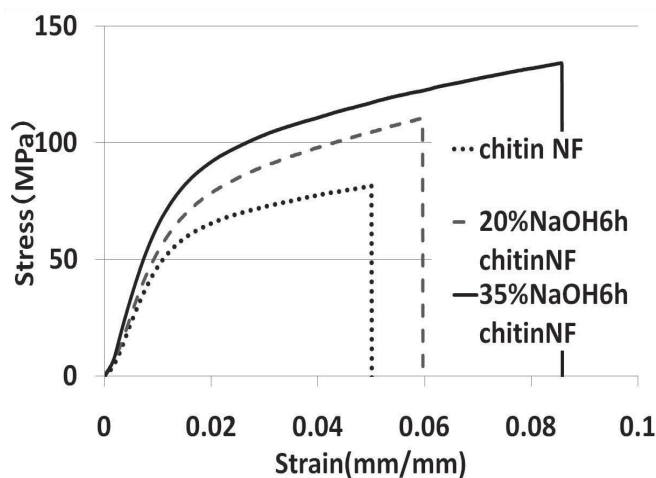| NaOH concentration	chitin	20%	35%	40%
DDA	0.06	0.24	0.54	0.84

Figure 1. Stress-strain curves of surface deacetylated chitin nanofiber sheet.

Development of New Bio-based Molded Products using Citric Acid.

(Graduate School of Agriculture, Laboratory of Sustainable materials, RISH, Kyoto University)

Tomohide Ueda

This study aims to develop a wood molded product using wood powder (*Acacia mangium*) and citric acid as a natural binder and to investigate its physical and mechanical properties.

The wood and citric acid powders were used as raw materials. The size of the wood powder was 60mesh pass (less than 250μm). The citric acid powder was mixed with the wood powder uniformly with the ratio of 0-40 wt%. The mixture was put into a mold and hot-pressed at 140~220°C with a pressure of 1~8MPa for 1~15min. The dark brown molded products were obtained as shown in Photo1. The densities of the products ranged from 0.9 to 1.3 g/cm^3. Three-point bending, water absorption, repeated boiling tests were performed to evaluate physical and mechanical properties of the molded products.

Figure 1 shows the bending properties of molded products. In the case of wood powder only, the bending properties of molded products were hardly indicated. The properties were improved with addition of citric acid, and the modulus of rupture (MOR) of 20wt% citric acid content reached a maximum value of 36MPa. The MOR value of molded products pressed at 180°C had about 39MPa. The molded products with citric acid did not decomposed even when a repeated boiling treatment. It was clarified that citric acid acted as a bio-adhesive.
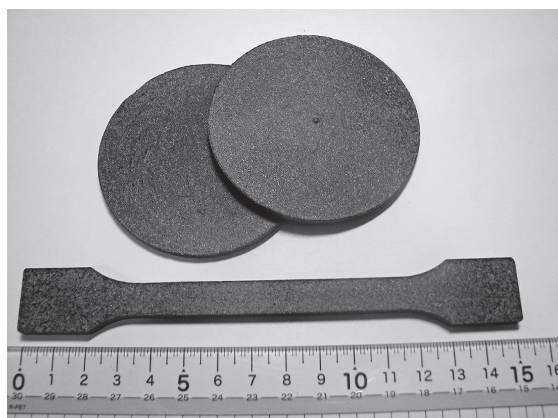
Photo1. The molded product consisting of wood and citric acid.
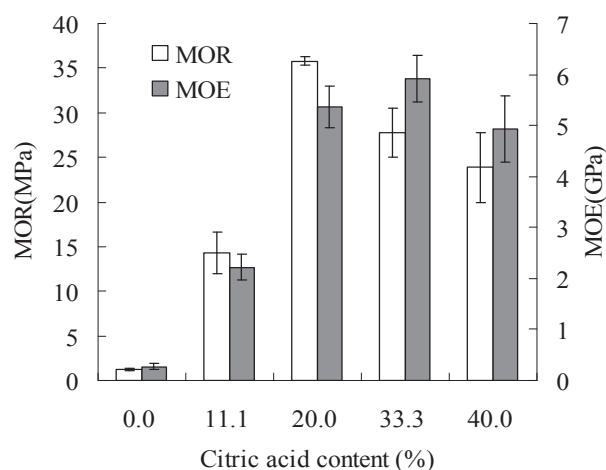

Figure1. Effects of CA content on the mechanical properties of molded product pressed at 200°C, 4MPa, for 10min.

Mechanical Analysis of the Failure Behavior on the Leg Joint in Wooden Portal Frame Structure

(Laboratory of Structural Function, RISH, Kyoto University)

Hiroyuki Nakatani

When wooden portal frame is subjected to the external force, a composite stress mixed with shear and moment occurs on its leg joint. In current Japanese design standard, check of the leg joint strength in wooden portal frame is done on both moment and shear force. If, however, shear force is dominant, split failure might occur dominantly. Unfortunately, however, any appropriate design equations for checking the split failure of joint has not been proposed yet, therefore the brittle behavior of this split failure is one of the serious problem in design of timber portal frame structures.

In this research, we focused on the influence of shear force that tends to bring split failure on the leg joint which was composed of Lagscrewbolt(LSB). LSB is screwed into the joint and connected by bolt with the other member, which leads to relatively high initial stiffness and strength. As one of the future research needs for the design of timber portal frame composed of LSB, consideration on split failure is necessary as described above because LSB itself tends to resist against shear force.

In this paper, we developed a mechanical model to predict the ultimate force when the leg joint fails by split. In this model, it was assumed that LSB was rigid body and also that it was rigidly connected with base steel member even if shear force and moment by external force are acted on the leg joint at a same time. Due to these assumptions, it was able to obtain the embedment stress distribution along the axis of LSB by superposition of triangular distribution stress derived from rotational moment and uniformly-distributed stress induced by shear force. Finally, we assumed that the split failure at leg joint will occur when tensile stress perpendicular to the grain which is equilibrium with this embedment stress reaches to a critical value.

The static lateral loading test whose shear span is enough short to be failed on split mode was carried out to obtain the shear strength. And the tensile thin plate test whose thickness is 50mm and the other parameter is same as the leg joint specimen was carried out to obtain the tensile strength perpendicular to the grain on the split failure, then substituting it into the model. Comparing the results on the lateral loading test to that calculated by the mechanical model, the validity of the modeling was confirmed to be reasonable.
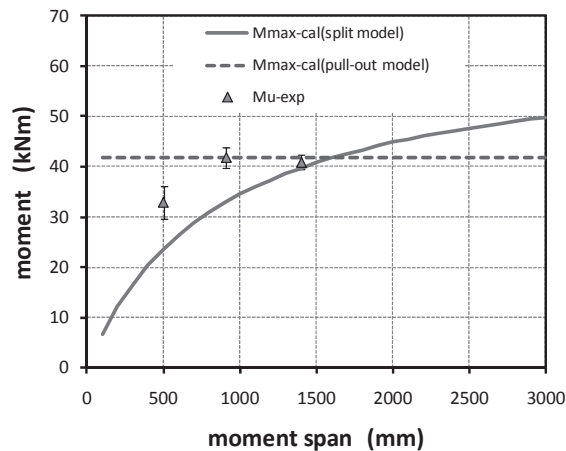
Figure. Test results of loading test on the joints and calculation for moment and moment span

Infestation and feeding biology of an invasive Lyctine beetle, *Lyctus africanus,* in Japan

(Laboratory of Innovative Humano-Habitability, RISH, Kyoto University)

Noriko Furukawa

In the postwar period, infestation by Lyctine beetles became a serious problem in Japan mainly because of the mass use of tropical broad-leaf timbers/plywood such as *Shorea* spp. for building materials, furniture and so on.   The most important species has been recognized as *Lyctus brunneus*. Recently, it is widely believed that infestation by Lyctine beetles is increasing with generalization of the super-insulated houses in Japan. The transition of Lyctine species is also likely to be one of the major reasons for this. The purposes of this research are to know the present major Lyctine species in Japan, and to compare feeding biology of important Lyctine species.

Firstly, a questionnaire survey together with the insect sample collection was conducted to all members of the Japan Termite Control Association (approx. 900 companies), some house builders and production companies of wood-based materials. Then all collected Lyctine samples were identified by their morphological characteristics. Of total 51 samples, the majority (33 samples) was identified as an invasive species, *Lyctus africanus*. Thirteen samples were attributed to *L. brunneus*, followed by *Minthea rugicollis* (3 samples), *L. linearis* (one sample) and *Lyctoxylon dentatum* (one sample). From the survey, it was clearly demonstrated that *L. africanus* was the major pest species in Lyctine in Japan these days, and is mainly distributed from Kyusyu area to Tokai area.

Secondary, feeding biology of *L. africanus* and *L. brunneus* was comparatively studied by the three test.

a) In the feeding preference test, sapwoods samples of *Shorea* sp*., Hevea brasiliensis, Tectona grandis, Quercus serrata, Castanea crenata, Juglans* sp*., Betula maximowicziana* and *Fraxinus mandshurica were* exposed to adults of *L. africanus* and *L. brunneus* for six months under the conditions of 26 °C and 60%RH, and the numbers of emerged insects (2nd generation) were counted as well as the observation of the samples by the Soft X-ray apparatus. After six months, only sapwood samples of *H. brasiliensis* were attacked by the both beetles. No feeding tunnels were observed in other samples, showing that female adults did not lay eggs to these sapwood samples.

b) Artificial diets consisting of soluble starch, wood powder and beer yeast were exposed to the mixed same numbers of adult pairs of *L. africanus* and *L. brunneus* under the conditions of 26 °C and 60%RH, and numbers and dates of emerged insects (2nd generation) from the diets were recorded daily for three months. Adults of *L. africanus* emerged from the diets earlier than those of *L. brunneus*, and the total numbers of emerged insects were significantly higher in *L. africanus* than in *L. brunneus*.

c) Artificial diets were separately exposed to the same numbers of adult pairs of *L. africanus* and *L. brunneus* under the conditions of 24°C, 26 °C and 28°C at 60%RH, and numbers and dates of emerged insects (2nd generation) from the diets were recorded daily for three months. Same as in the mixed species test, adults of *L. africanus* emerged earlier than those of *L. brunneus* at any temperatures. Interestingly, the numbers of total emerged adults were increased with temperature in *L. africanus,* and on the contrary, they were decreased with temperature in *L. brunn*eus. This may show the different temperature preference of these two Lytine species, which has relationship with their distribution.

These results suggest that *L. africanus* must win the competition with *L. brunneus* in the near future in Japan*,* and that the standards and test methods, which have been developed against *L. brunneus*, have to be revised by considering feeding biology of *L. africanus*.

Acknowledgements

Research of a power transmitting and receiving system on microwave wireless charging for an electric vehicle

(Graduate School of Technology, Laboratory of Computer Experiment for Sustainable Humanosphere, RISH, Kyoto University)

Masayuki Koizumi

Our research group has been studying on wireless power transmission systems by microwave for electric vehicle charging. In these systems, microwave power is transmitted from slot antennas on the ground to rectennas on the bottom of the vehicle. The rectenna is composed of a patch antenna and a rectifying circuit. The rectennas receive microwave and rectify it to DC power, and DC power is supplied to capacitors. The objective of the present study is to improve charging efficiency.

We found out if enough antennas covered the slot antenna's radiation area, the transmitting efficiency remained only 50% in simulation. Then, we tried to improve transmitting efficiency among transmission and receiving antennas. We used slot antennas of 45cm long and a miniature car, to simplify the experimental system. We designed a slot antenna and a patch antenna having high performance under proximally location. Antennas' performance gets worse other antennas' influence in proximally location. It caused by change of impedance of the transmitting space. So, we changed the antennas' input impedance and output impedance by shifting slot position and feeding position. According to this improve, transmitting efficiency improved to 53.7% from 47.4% in simulation.

Next, we invented receiving unit with obliquely placed patch antennas (Fig.1). The microwave from the slot antenna expands in a radial fashion in near field, and enters the side of patch antennas obliquely. But it can't be received well, because of patch antennas' directivity. Therefore, we set antennas of side part at an angle to match the receiving directivity of patch antennas and radiation directivity of a slot antenna. Using this receiving unit, transmitting efficiency goes up to 84.4% in simulation (Fig.2).

Figure 2. Simulation result of microwave propagation between transmitting and receiving antenna.

Based on the simulation, we carried out an experiment, and get 76.0% of transmitting efficiency. As a result, the overall charging efficiency from waveguide to capacitor improved to 33%, 12% higher than that of the last experiments.
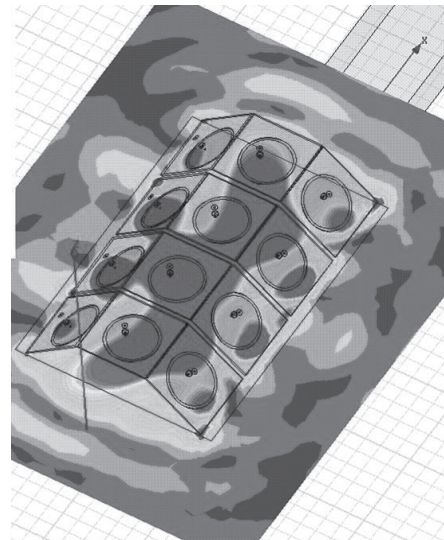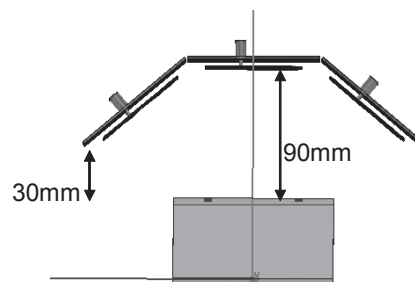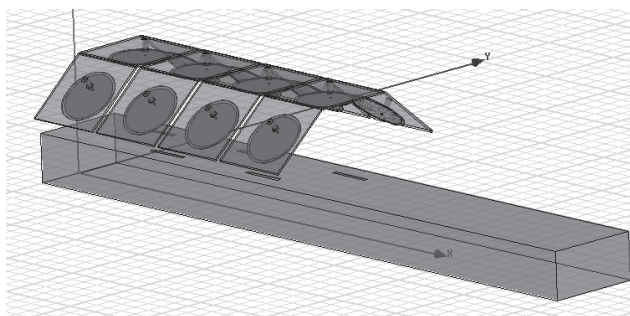

Figure 1. Oblique receiving unit (rectenna) which increases the transmitting efficiency of 84.4%

Electronstatic Solitary Waves observed by KAGUYA

**(Graduate School of Technology,
Laboratory of Applied Radio Science for Sustainable Humanosphere,
RISH, Kyoto University)**

Maki Hashitani

We observed electrostatic solitary waves (ESW) near the Moon by SELENE (KAGUYA) in the solar wind and in the lunar wake. SELENE is a lunar orbiter with an altitude of 100km and measured wave electric field, background magnetic field, and fluxes of ions and electrons. ESW observations are categorized into three types depend on the observed conditions: ESW generated by the electric in the wake boundary (Type A), strong ESW generated by the solar wind and bi-streaming electrons mirror-reflected over the magnetic anomaly (Type B), and ESW generated by the solar wind and counter-streaming electrons reflected back from the lunar surface (Type C). ESW of Type C often alternate with Langmuir waves.

Type A ESW at the wake boundaries are generated far from the Moon and they propagate along the magnetic field to the SELENE orbits. The energetic electrons accelerated by the strong electric at the wake boundary move along the magnetic field line, resulting in the bump-on-tail instability. A series of potentials due to the instability coalesce with each other to form

Figure 1. Electrostatic solitary waves observed above a magnetic anomaly.

larger and longer solitary potentials through propagation along the magnetic field. The longer distance of propagation in the wake boundary makes the magnitude of ESW comparable to those due to the strong bi-stream instability occurring in the short distance above the dayside magnetic anomalies. Total field strengths of magnetic anomalies at the surface of the Moon as derived from the Lunar Prospector electron reflectometer experiment reach more than 40 nT. Because of the strong magnetic field new the Moon

surface, a substantial amount of electrons are reflected at mirror points above the anomalies, and they are observed by SELENE when the magnetic field are connected to the Moon. The Langmuir waves or ESW are alternately observed in Type C ESW events. Since the electron reflection over the surface without magnetic anomalies is relatively weak, a weak beam is formed. resulting in the weak-beam instability or the bump-on-tail instability. Either Langmuir waves or ESW are generated depending on the background electron and ion thermal velocities.
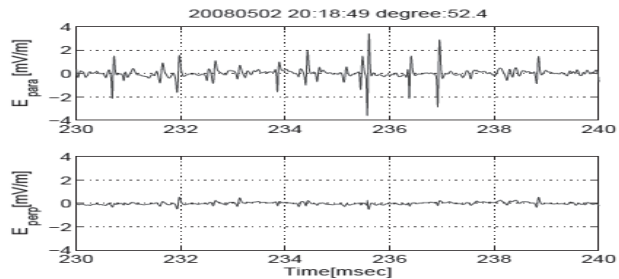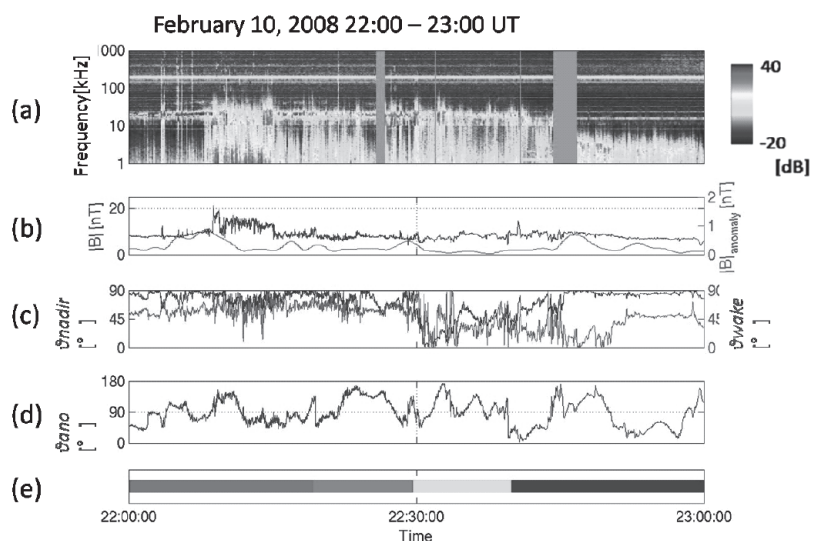

Figure 2. Plasma wave observation over a magnetic anomaly. (a) electric field spectra, (b) magnetic field intensity, (c) magnetic field intensity, (c) (d) magnetic field direction, (e) location of spacecraft.

Miniaturization and Integration of the System for measuring Space Electromagnetic Environments

(Graduate School of Engineering, Laboratory of Space Systems and Astronautics, RISH, Kyoto University)

Hajime Fukuhara

Since space plasmas are essentially collisionless, kinetic energies of plasma particles are exchanged through the plasma waves. These interactions among the space plasmas and the plasma waves are called the wave-particle interactions. The wave-particle interactions are very important in analyzing electromagnetic phenomena occurring in space. A number of scientific satellites have been launched to measure space electromagnetic environments. We address two themes in the present paper as follows: (i) development of the one-chip type of a new system for measuring the wave-particle interactions, (ii) miniaturization of analog parts of the plasma wave receivers.

The Wave-Particle Interaction Analyzer (WPIA) is a novel instrument to observe wave-particle interactions directly by calculating the inner product between the electric field of plasma waves and of plasma particles. The WPIA has four fundamental functions: waveform calibration, coordinate transformation, time correction, and interaction calculation. We demonstrate the feasibility of One-chip WPIA (O-WPIA) using a Field Programmable Gate Array (FPGA) as a test model for future science missions. The O-WPIA is capable of real-time processing with low power consumption. We validate the performance of the O-WPIA including determination of errors in the calibration and power consumption.

We also develop a tiny chip using analog ASIC (Application Specific Integrated Circuit) technology for scientific and extra objectives [1]. The package size is 15 mm times 15 mm, and it contains the bare chip with the size of 3 mm £ 3 mm shown in figure 1. The chips are manufactured with CMOS 0.25 μm process by TSMC Co., Ltd. Several types of analog filters and amplifiers are implemented in the chip. We design the Gm-C filter, the SC (Switched Capacitor) filters, and the differential amplifier. The Gm-C filter is realized with OTA (Operational Transconductance Amplifier) and capacitors. The frequency response of the Gm-C filter is compensated within ±1 % in the -30 to 60 degrees C range by the compensation circuits [2]. We design six channels of waveform receivers inside a single chip. Figure 2 shows a mask pattern layout of the six-channel waveform receiver. The circuits and I/O pad are implemented inside the size of 3 mm times 3 mm.
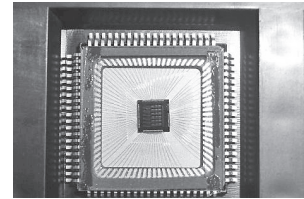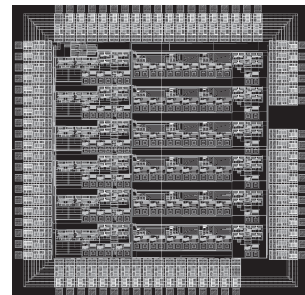

Figure 1. The photograph of the ASIC.

Figure 2. The layout of the waveform receiver.

Acknowledgements

References

[1] Kojima, H., H. Fukuhara, Y. Mizuochi, S. Yagitani,H. Ikeda, Y. Miyake, H. Usui, H. Iwai, Y. Takizawa, Y. Ueda and H. Yamakawa, "Miniaturization of plasma wave receivers onboard scientific satellites and its application to the sensor network system for monitoring the electromagnetic environments in space," *Adv. in Geosci.*, vol.21, pp.461-481, 2010.

[2] Agawa, K., Majima, H., Kobayashi, H., Koizumi,M., Ishizuka, S., Nagano, T., Arai, M., Shimizu, Y.,Urakawa, G., Itoh, N., Hamada, M., and Otsuka, N., "A ¡90 dBm Sensitivity 0.13 ¹m CMOS Bluetooth Transceiver Operating in Wide Temperature Range," *Proc. IEEE Custom Integr. Circuits Conf.*, vol.2, pp.655-658, 2007.